Antitumor Activity of Py-Im polyamides

Thesis by

Fei Yang

In Partial Fulfillment of the Requirements
For the Degree of
Doctor of Philosophy

California Institute of Technology
Pasadena, California
2014
(Defended July 8th, 2013)

For my family

Acknowledgement

I would like to thank Professor Peter Dervan for his guidance over the past five years. I am especially grateful for the latitude he has given me to pursue new ideas, and for his continued support after many of those ideas led to dead ends. The skills I've learned from the numerous training opportunities he has provided will be instrumental as I navigate my career in science.

Being at Caltech, I've had the opportunity to work with very capable individuals, many of whom I've had the good fortune to collaborate with. Georgi, John, Ben, Jerzy, Jordan, and Jamie, I thank you all for your contributions. In particular, I would like to acknowledge Nick Nickols, who has been my collaborator since the beginning of the animal projects. Our many discussions over hookah helped shape the direction of the work presented herein.

Most of all, I thank my family, without their support this work would not be possible.

Abstract

Molecules that inhibit DNA dependent processes are the most commonly used agents for the treatment of cancer. The genotoxicity associated with their mechanisms of action, unfortunately, make them extremely toxic to the patient and cancer cells alike. The work presented in this thesis outlines the development of Py-Im polyamides as non-genotoxic DNA-targeted antitumor molecules that interfere with RNA polymerase II elongation. We initially characterized the pharmacokinetic profiles of two hairpin polyamides to establish their bioavailability in the serum and tissues after a single administration. We next determined the molecular mechanism that contributes to toxicity of a hairpin polyamide in human prostate cancer cells in cell culture and we demonstrated antitumor effects of the compound against LNCaP xenografts in mice. Finally, we conducted animal toxicity experiments on 4 polyamides that vary on the γ-turn with respect to the substitution of amino and acetamide groups at the α and β positions. From this study we identified a second generation compound that retains antitumor activity with significantly reduce animal toxicity. This work sets the foundation for the development of Py-Im polyamides as DNA targeted therapeutics for the treatment of advanced prostate cancer.

Table of Contents

List of Figures and Tables……vii

Chapter 1: Introduction: DNA as a therapeutic target in cancer……...……1

Chapter 2: Single-dose pharmacokinetic and toxicity analysis of pyrrole imidazole polyamides in mice……..…….14

Chapter 3: Antitumor activity of a pyrrole-imidazole polyamide……..….36

Chapter 4: Animal toxicity of hairpin pyrrole-imidazole polyamides varies with the turn unit ……59

List of figures and tables

Chapter 1

Figure 1.1. Transcription and replication dependent mechanisms of DNA repair……..3

Table 1.1. Selection of FDA approved compounds……4

Figure 1.2. Select noncovalent sequence specific minor groove binders……7

Figure 1.3. Sequence recognition by hairpin Py-Im polyamides……8

Chapter 2:

Figure 2.1. Chemical structures and plasma concentration of polyamides……22

Table 2.1. Plasma pharmacokinetic parameters……..…….23

Figure 2.2. Urinary and fecal excretion of polyamides…….……24

Figure 2.3. Tissue distribution of polyamides……...25

Table 2.2. Tissue pharmacokinetic parameters…….…….26

Figure 2.4. Animal toxicity of polyamides…….……..27

Figure S2.1. Chemical structures of polyamide standards…..…….34

Figure S2.2. Stability of polyamides…….……35

Chapter 3:

Figure 3.1. Chemical structures of polyamides **1** and **2**……..……...…39

Figure 3.2. Global effect of **1** on RNAP2……45

Figure 3.3. Cytotoxicity of polyamides **1** and **2** in LNCaP cells……47

Figure 3.4. Effects of polyamide **1** on cellular DNA damage response…….48

Figure 3.5. Effects of polyamide **1** on human prostate cancer xenografts……...49

Figure S3.1. Heat map of global distribution of RNAP2 over gene bodies……...56

Figure S3.2. Cytotoxcity and cell uptake of polyamides **1** and **2**……...57

Figure S3.3. Circulation of polyamide **1**……...58

Figure S3.4. Animal weights after polyamide treatment……..…58

Table S3.1. Primer sequences used in study…….58

Chapter 4:

Figure 4.1. Chemical structures of polyamides **1-4**…….62

Figure 4.2. Experiment set up of single dose weight curve experiments……69

Figure 4.3. Histopathology analysis and serum

chemistry of animals treated with **1-4**.....72

Figure 4.4. Experiment set up of multi dose weight curve experiments……74

Figure 4.5. Activity of **3** in LNCaP cells……76

Figure 4.6. Activity of **3** against LNCaP xenografts……..77

Table S4.1. MALDI-ToF analysis of compounds…….……86

Figure S4.1. DNA thermal stabilization of **1-4**……86

Figure S4.2. Serum circulation of **1-4**……...87

Figure S4.3. Characterization of cyclic polyamide **5**……88

Table S4.2. Microsomal stability of **1-4**……89

Figure S4.4. Chemical structures of **6-9**……..90

Figure S4.5. Nuclear localization of **6-9** in the liver……90

Chapter 1

Introduction: DNA as a therapeutic target in cancer

1.1 Background and significance.

The human genome consists of approximately 20,000 protein coding genes and many more genes that encode non-coding RNA with crucial cellular functions.(1) The regulatory networks that govern gene expression are immensely complex and work cooperatively to control cellular function and cellular response to environmental stimuli. It is due to this intricate regulation of gene expression that cells of the same genetic material can differentiate into various phenotypes in the human body to perform specialized tasks.

As a result of numerous DNA dependent processes, corruption to the DNA code can result in aberrant cellular behavior.(2) Thus, essential DNA dependent processes such as transcription and replication participate in DNA damage repair to ensure genomic stability.(3, 4) (Fig. 1.1) Transcription coupled nucleotide excision repair (TC-NER) is a mechanism that relies on elongating RNA polymerase II (RNAP2) to identify lesions or blockages in the DNA. Once the RNAP2 holoenzyme encounters a blockage on the transcribed DNA strand it recruits the proteins CSA, CSB, XAB2, and HMGN1 to repair the DNA lesion. If the DNA damage cannot be repaired, persistent blockage to RNAP2 elongation will trigger p53 dependent and independent apoptosis.(3, 5-8) Similarly, DNA lesions are recognized by replicating DNA polymerase in the S phase.(4) If the lesion cannot be repaired, persistent block to replication will also trigger cell death. While most instances of DNA damage are efficiently repaired, some escape as mutations and are retained in the genetic code. Over time these mutations accumulate and cause altered patterns of gene expression, which ultimately lead to genetic diseases like cancer.

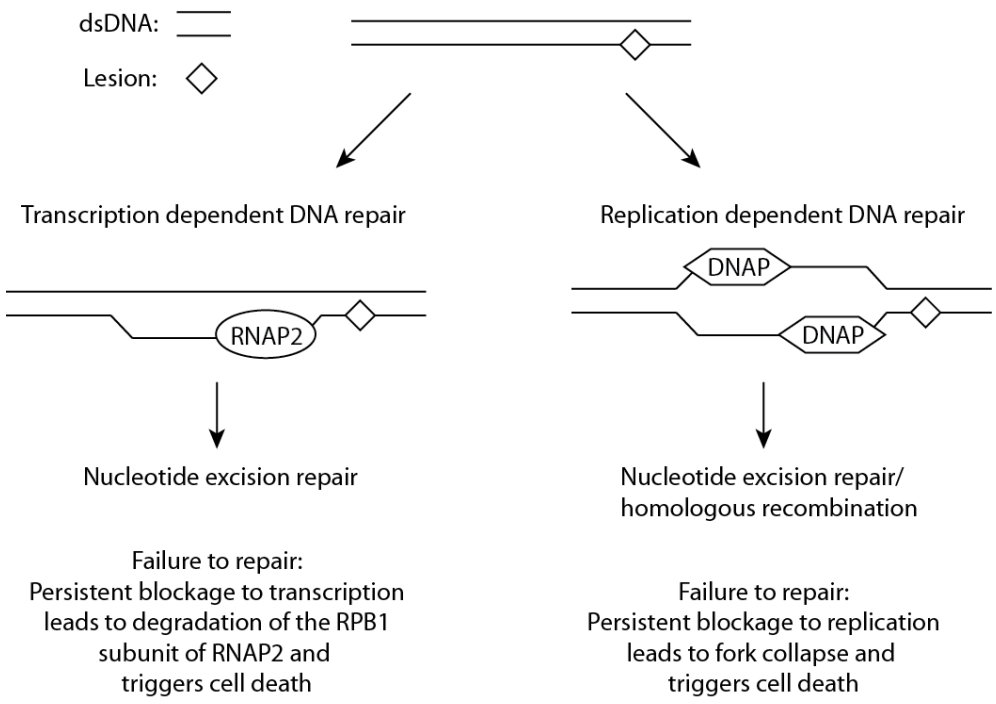

Figure 1.1. Transcription and replication dependent mechanisms of DNA repair.

1.2 DNA as a target for cancer therapy.

As the underlying source of cancer, some of the oldest and most effective anticancer agents are targeted to the DNA. Historically, the development of DNA targeted chemotherapeutics began as circumstantial observation to the side effects of chemical warfare during World War II.(9) Physicians examining sailors exposed to mustard gas, after a shipment of M47A1 mustard gas bombs leaked from the damaged *SS John Harvey,* noticed signs of lymphoid and myeloid suppression.(10) It was reasoned that the high proliferation rate of bone marrow cells made them susceptible to the alkylating effects of mustard gas, thus cancers with similarly high proliferations rates, such as leukemias and lymphomas, may also be targeted by such agents.(11) In a clinical study by Goodman et al. in 1946, it was found that treatment with nitrogen mustards indeed caused remission in patients with lymphoma.(12)

Intercalation Binding Compound	Selectivity	Action	Clinical use
Daunomycin	5'-WCG	inhibition of topoisomerase II	acute myeloid leukemia
Doxorubicin	5'-WCG	inhibition of topoisomerase II	breast cancer, stomach cancer, cervical cancer, non-Hodgkin's lymphoma, adult acute leukemia, endometrial cancer, rhabdomyosarcoma
Idarubicin	5'-WCG	inhibition of topoisomerase II	acute myeloid leukemia
Epirubicin	5'-WCG	inhibition of topoisomerase II	breast cancer
Actinomycin D	5'-PyGCPu	inhibition of topoisomerase II	Ewing's sarcoma, Wilms' tumors, soft-tissue sarcomas
Topotecan	ND	inhibition of topoisomerase I	ovarian, lung, cervical cancer
Irinotecan	ND	inhibition of topoisomerase I	ovarian, lung, cervical cancer
Etoposide	ND	inhibition of topoisomerase II	testicular cancer, small-cell lung cancer
Teniposide	ND	inhibition of topoisomerase II	acute lymphocytic leukemia
Mitoxantrone	5'-PuPy	inhibition of topoisomerase II	leukemias, breast cancer, ovarian cancer, prostate cancer
Minor Groove Binding			
Bleomycin	5'-GC, 5'-GT	ds DNA cleavage	testicular cancer, non-Hodgkin's lymphoma
Mitomycin C	5'-CG	alkylation/crosslinking	stomach, gi, anal, bladder, breast, cervical, colorectal, head and neck, and non-small cell lung cancer
Mithramycin	GC-rich	inhibits RNA synthesis	testicular cancer
Other			
Cisplatin	ND	crosslinking	testicular, ovarian, head and heck cancers
Temozolomide	ND	alkylation	astrocytoma and melanoma
Decitabine	ND	DNMT inhibitor	acute myeloid leukemia, medulloblastoma
5-fluoruracil	ND	thmyidylate synthase inhibitor	colon, recturm, head and neck cancers
Cytarabine	ND	inhibits DNA and RNA synthesis	acute myeloid leukemia

Table 1.1. Selection of FDA approved compounds that affect DNA dependent processes.[13, 14]

The utility of alkylating agents for the treatment of lymphoma opened the way for the development of new DNA targeted agents with novel mechanisms.(13, 14) (Table 1.1) Many of these drugs form covalent interstrand crosslinks, stabilize protein-DNA complexes of topoisomerases I and II, or inhibit DNA and RNA synthesis.(4, 13, 14) These modifications to the DNA introduce blockages to many DNA dependent processes including transcription and replication, which in turn triggers apoptosis in diseased cells.(4, 14-17) However, because transcription and replication are common to cancerous

and normal cells alike, systemic treatment with DNA targeted therapeutics can be very toxic to the patient as well.

1.3 Limitations of DNA targeted therapy.

Most DNA targeted therapeutics preferentially affect cancerous cells due to their high proliferation rate and genomic instability, but benign cells can also be affected. Normal cells can tolerate basal levels of DNA damage generated by exogenous chemicals and by by-products of cellular metabolism. However, the endogenous DNA repair mechanisms are often overwhelmed by DNA targeted therapeutics.(18) Studies of patients treated daunomycin and cytarabine shortly after their introduction in the 1960s documented the presence chromosomal abnormalities associated with DNA fragmentation in normal cells.(19, 20) The extensive DNA damage caused by chemotherapeutic treatment has been linked to the acquisition of resistance towards chemotherapy and the development of secondary cancers.(21-23)

A recent study on the effects of chemotherapy in the tumor microenvironment indicates genotoxic stress can cause normal cells to promote tumor survival, which further complicates the long term utility of DNA targeted drugs. In the study by Sun et al. treatment of prostate fibroblasts with DNA damaging agents such as bleomycin, mitoxantrone, and ionizing radiation was found to activate WNT16B expression in a NF-κB dependent manner.(24) Interestingly, the expression of WNT16B was not significantly increased when prostate cancer cells were treated with the same genotoxic agents. As a secreted signaling protein, WNT16B activates the Wnt expression program in tumor cells, which in turn promotes survival and metastasis.

As a consequence of the numerous side effects of DNA targeted therapeutics, research in the field has waned in favor of therapeutic agents with more specific molecular targets and less systemic toxicity.(14) However, despite their limitations DNA targeted therapies remain a staple in most treatment regimens. Thus, development of a new class of DNA targeted molecules, without genotoxic side effects, could circumvent the problems associated with current therapies.

1.4 Noncovalent minor groove binders as anticancer agents.

DNA minor groove binders consist of molecules that permanently modify DNA in a covalent manner and those that interact with DNA noncovalently. The latter group of molecules interferes with DNA dependent process in a reversible manner. This group of molecules includes DAPI, pentamidine, berenil, Hoechst, distamycin A, netropsin, and their synthetic derivatives.(25)

Clinically, diarylamidines, consisting of DAPI, pentamidine, and berenil, have been used for the treatment of several protozoa related diseases.(26) (Fig. 1.2) The minor groove binder DAPI inhibits DNA and RNA polymerases by binding to A/T rich tracts of DNA.(27-30) While DAPI is active against *Trypanosome Congolese,* undesirable side effects have limited its clinical use. Pentamidine is clinically used to treat infections of *Trypanosoma brucei gambiense*, *Leismania donovani*, and *Pneumocystis carinii*. Berenil is used to treat trypanosomiasis in veterinary medicine.(25)

Bisbenzimidazoles are Hoechst-like compounds that bind to A/T rich DNA sequences.(31, 32) (Fig. 1.2) They have been shown to interfere with DNA dependent process in cell culture without causing DNA damage.(33) Furthermore, a symmetric

bisbenzimidazole has demonstrated antitumor activity against CH1 human ovarian carcinoma xenografts *in vivo*.(34)

Distamycin A and netropsin are tripyrrole and dipyrrole oligomers, respectively, and bind to A/T tracts. Both compounds bind to the minor groove in a 1:1 fashion.(35, 36) (Fig. 1.2) Distamycin has been shown to also bind in a 2:1 manner.(37) Similar to other noncovalent minor groove binders, these compounds inhibit DNA and RNA polymerases.(6, 28, 38)

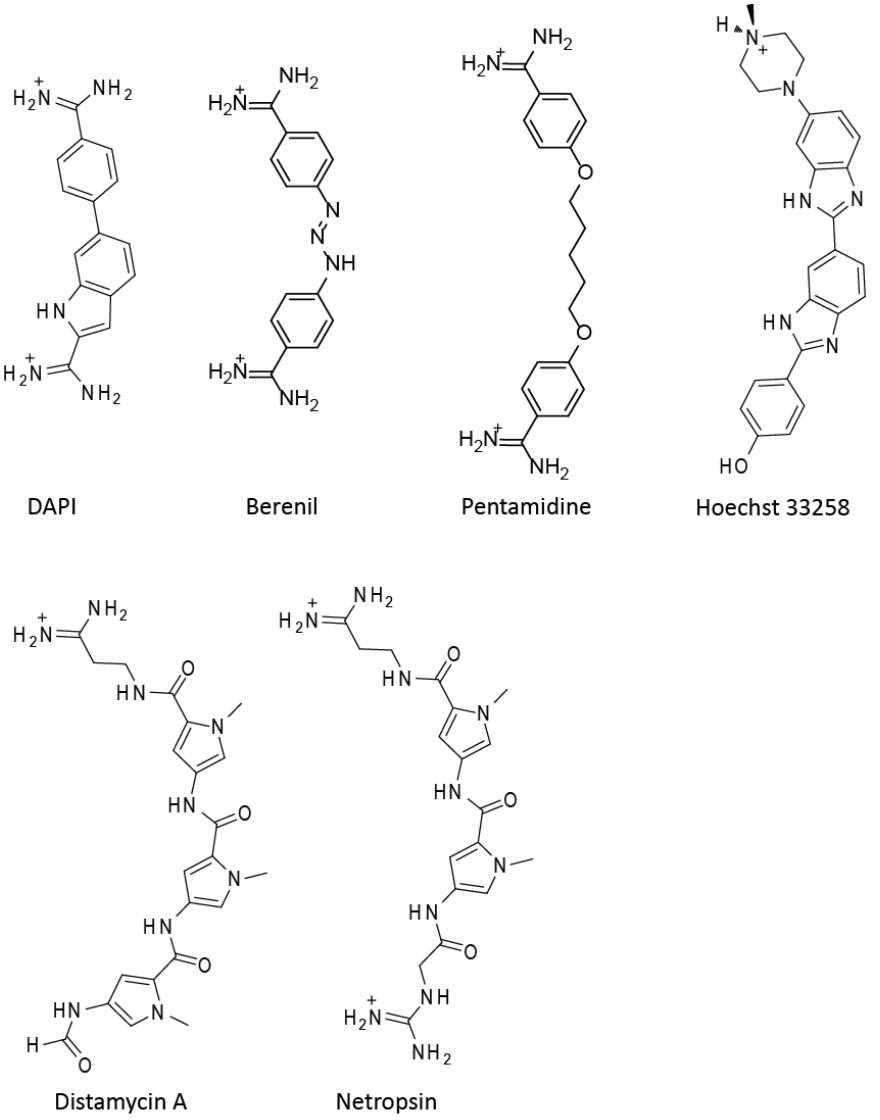

Figure 1.2. Select noncovalent sequence specific minor groove binders.

Py-Im polyamides are synthetic oligomers based on the structures of distamycin A and netropsin. Research in the Dervan lab have improved the DNA binding affinity of polyamides by linking two oligomers with a turn unit and enforcing 2:1 binding as a hairpin.(39) Sequence recognition by polyamides has also been expanded by incorporation of new aromatic heterocycles that discriminate between A/T and G/C base pairs through the antiparallel pairing of these amino acids.(40, 41) (Fig. 1.3) Additionally, conjugation of fluorescein or isophthalic acid to the C-terminal tail of polyamides significantly improves their nuclear localization.(42, 43)

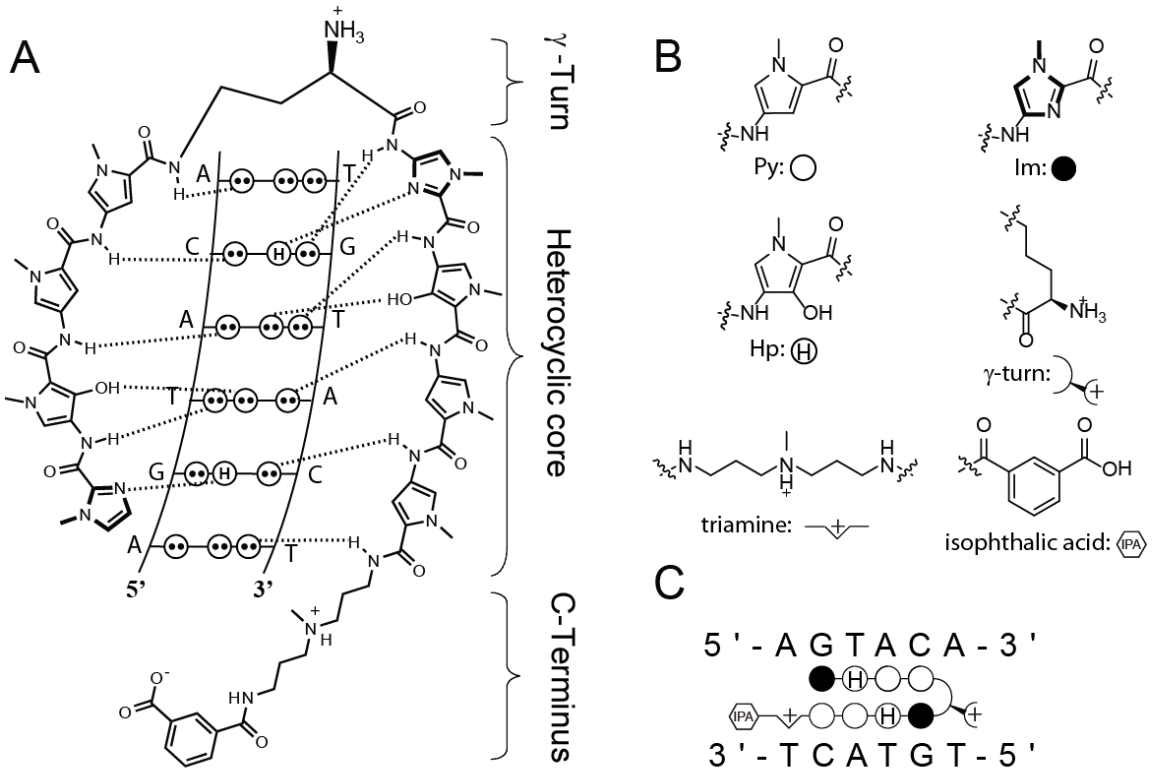

Figure 1.3. Sequence recognition by hairpin Py-Im polyamides. **(A)** DNA base pair discrimination on the minor groove floor is achieved by the antiparallel pairing of aromatic heterocycles. Py/Im pairing recognizes G/C base pairing, Hp/Py pairing recognizes T/A pairing, and Py/Py pairing is degenerate for T/A or A/T. The γ-turn and the c-terminus tail are degenerate for T/A or A/T. **(B)** Ball and stick representation of hairpin components. **(C)** A ball and stick representation of a polyamide bound to its target sequence.

Historically, these compounds were found to exhibit antifungal activity in yeast through a DNA dependent mechanism that did not cause genotoxicity.(44) In cell culture, Py-Im polyamides are able to regulate gene expression in inducible transcription systems(45-49), and are toxic to a variety of cancer cell lines.(50) Animal experiments have shown Py-Im polyamides are bioavailable through multiple forms of administration(51-55), and can affect gene expression in target tissues *in vivo*.(56, 57) These characteristics make Py-Im polyamides ideal candidates for development as novel DNA targeted therapeutics.

1.5 Scope of this work.

The work presented here focuses on the characterization of Py-Im polyamides as non-genotoxic antitumor agents that are active against prostate cancer xenografts. Chapter 2 details the pharmacokinetic and animal toxicity analysis of two hairpin polyamides targeted to the 5'-WGWWCW-3' sequence found in the androgen response element. In this study it was found that the polyamide with an α amino turn was much less toxic to animals than the compound with a β acetamide turn.(55) The less toxic polyamide is further characterized in chapter 3 as a non-genotoxic DNA binder that interferes with RNAP2 elongation, and causes cell death in human prostate cancer cells in cell culture and in xenografts.(58) Chapter 4 revisits the difference in rodent toxicity that stems from the γ-turn. By using 4 polyamides that vary at the turn (α amino, β amino, α acetamide, and β acetamide), we assessed differences in animal toxicity and determined the target organs of pathology. From this study we identified a structural analog to the parent compound that retains antitumor activity without causing animal toxicity.

References

1. International Human Genome Sequencing C (2004) Finishing the euchromatic sequence of the human genome. *Nature* 431(7011):931-945.
2. Bywater MJ, Pearson RB, McArthur GA, & Hannan RD (2013) Dysregulation of the basal RNA polymerase transcription apparatus in cancer. *Nat Rev Cancer* 13(5):299-314.
3. Aune GJ*, et al.* (2008) Von Hippel-Lindau - Coupled and Transcription-Coupled Nucleotide Excision Repair - Dependent Degradation of RNA Polymerase 11 in Response to Trabectendin. *Clinical Cancer Research* 14(20):6449-6455.
4. Sancar A, Lindsey-Boltz LA, Unsal-Kacmaz K, & Linn S (2004) Molecular mechanisms of mammalian DNA repair and the DNA damage checkpoints. *Annual review of biochemistry* 73:39-85.
5. Arima Y*, et al.* (2005) Transcriptional blockade induces p53-dependent apoptosis associated with translocation of p53 to mitochondria. *Journal of Biological Chemistry* 280(19):19166-19176.
6. Zhang Z*, et al.* (2009) Tanshinone IIA triggers p53 responses and apoptosis by RNA polymerase II upon DNA minor groove binding. *Biochem Pharmacol* 78(10):1316-1322.
7. Derheimer FA, Chang CW, & Ljungman M (2005) Transcription inhibition: A potential strategy for cancer therapeutics. *European Journal of Cancer* 41(16):2569-2576.
8. Turinetto V*, et al.* (2009) The cyclin-dependent kinase inhibitor 5, 6-dichloro-1-beta-D-ribofuranosylbenzimidazole induces nongenotoxic, DNA replication-independent apoptosis of normal and leukemic cells, regardless of their p53 status. *BMC cancer* 9:281.
9. Kohn KW (1996) Beyond DNA cross-linking: history and prospects of DNA-targeted cancer treatment--fifteenth Bruce F. Cain Memorial Award Lecture. *Cancer research* 56(24):5533-5546.
10. Faguet GB (2005) *The War on Cancer* (Springer).
11. Gilman A & Philips FS (1946) The biological actions and therapeutic applications of the B-chloroethyl amines and sulfides. *Science* 103(2675):409-415.
12. Goodman LS, Wintrobe MM, & et al. (1946) Nitrogen mustard therapy; use of methyl-bis (beta-chloroethyl) amine hydrochloride and tris (beta-chloroethyl) amine hydrochloride for Hodgkin's disease, lymphosarcoma, leukemia and certain allied and miscellaneous disorders. *Journal of the American Medical Association* 132:126-132.
13. Tse WC & Boger DL (2004) Sequence-selective DNA recognition: natural products and nature's lessons. *Chemistry & biology* 11(12):1607-1617.
14. Hurley LH (2002) DNA and its associated processes as targets for cancer therapy. *Nature reviews. Cancer* 2(3):188-200.
15. Jung Y & Lippard SJ (2006) RNA polymerase II blockage by cisplatin-damaged DNA - Stability and polyubiquitylation of stalled polymerase. *Journal of Biological Chemistry* 281(3):1361-1370.

16. Kopka ML, Yoon C, Goodsell D, Pjura P, & Dickerson RE (1985) The molecular origin of DNA-drug specificity in netropsin and distamycin. *Proceedings of the National Academy of Sciences of the United States of America* 82(5):1376-1380.
17. Ljungman M, O'Hagan HM, & Paulsen MT (2001) Induction of ser15 and lys382 modifications of p53 by blockage of transcription elongation. *Oncogene* 20(42):5964-5971.
18. Fojo T (2001) Cancer, DNA repair mechanisms, and resistance to chemotherapy. *Journal of the National Cancer Institute* 93(19):1434-1436.
19. Bell WR, Whang JJ, Carbone PP, Brecher G, & Block JB (1966) Cytogenetic and Morphologic Abnormalities in Human Bone Marrow Cells during Cytosine Arabinoside Therapy. *Blood-J Hematol* 27(6):771-&.
20. Whang-Peng J, Leventhal BG, Adamson JW, & Perry S (1969) The effect of daunomycin on human cells in vivo and in vitro. *Cancer* 23(1):113-121.
21. Arseneau JC*, et al.* (1972) Nonlymphomatous malignant tumors complicating Hodgkin's disease. Possible association with intensive therapy. *The New England journal of medicine* 287(22):1119-1122.
22. Karran P (2001) Mechanisms of tolerance to DNA damaging therapeutic drugs. *Carcinogenesis* 22(12):1931-1937.
23. Salehan MR & Morse HR (2013) DNA damage repair and tolerance: a role in chemotherapeutic drug resistance. *British journal of biomedical science* 70(1):31-40.
24. Sun Y*, et al.* (2012) Treatment-induced damage to the tumor microenvironment promotes prostate cancer therapy resistance through WNT16B. *Nat Med* 18(9):1359-+.
25. Baraldi PG*, et al.* (2004) DNA minor groove binders as potential antitumor and antimicrobial agents. *Med Res Rev* 24(4):475-528.
26. Dann O*, et al.* (1972) [Trypanocidal diamidines with three rings in two isolated ring systems]. *Justus Liebigs Annalen der Chemie* 760(761):37-87.
27. Mildner B, Metz A, & Chandra P (1978) Interaction of 4'-6-diamidino-2-phenylindole to nucleic acids, and its implication to their template activity in RNA-polymerase reaction of E. coli bacteria and of Friend-virus infected mouse spleen. *Cancer letters* 4(2):89-98.
28. Brosh RM, Jr.*, et al.* (2000) Potent inhibition of werner and bloom helicases by DNA minor groove binding drugs. *Nucleic acids research* 28(12):2420-2430.
29. Parolin C*, et al.* (1990) The effect of the minor groove binding agent DAPI (4,6-diamidino-2-phenyl-indole) on DNA-directed enzymes: an attempt to explain inhibition of plasmid expression in Escherichia coli [corrected]. *FEMS microbiology letters* 56(3):341-346.
30. Larsen TA, Goodsell DS, Cascio D, Grzeskowiak K, & Dickerson RE (1989) The structure of DAPI bound to DNA. *Journal of biomolecular structure & dynamics* 7(3):477-491.
31. Wood AA, Nunn CM, Czarny A, Boykin DW, & Neidle S (1995) Variability in DNA Minor-Groove Width Recognized by Ligand-Binding - the Crystal-Structure of a Bis-Benzimidazole Compound Bound to the DNA Duplex D(Cgcgaattcgcg)(2). *Nucleic acids research* 23(18):3678-3684.

32. Clark GR, Boykin DW, Czarny A, & Neidle S (1997) Structure of a bis-amidinium derivative of hoechst 33258 complexed to dodecanucleotide d(CGCGAATTCGCG)2: the role of hydrogen bonding in minor groove drug-DNA recognition. *Nucleic acids research* 25(8):1510-1515.
33. Kim SO*, et al.* (2013) STK295900, a dual inhibitor of topoisomerase 1 and 2, induces G(2) arrest in the absence of DNA damage. *PloS one* 8(1):e53908.
34. Mann J*, et al.* (2001) A new class of symmetric bisbenzimidazole-based DNA minor groove-binding agents showing antitumor activity. *Journal of medicinal chemistry* 44(2):138-144.
35. Coll M, Frederick CA, Wang AH, & Rich A (1987) A bifurcated hydrogen-bonded conformation in the d(A.T) base pairs of the DNA dodecamer d(CGCAAATTTGCG) and its complex with distamycin. *Proceedings of the National Academy of Sciences of the United States of America* 84(23):8385-8389.
36. Zimmer C & Wahnert U (1986) Nonintercalating DNA-Binding Ligands - Specificity of the Interaction and Their Use as Tools in Biophysical, Biochemical and Biological Investigations of the Genetic Material. *Prog Biophys Mol Bio* 47(1):31-112.
37. Pelton JG & Wemmer DE (1989) Structural characterization of a 2:1 distamycin A.d(CGCAAATTGGC) complex by two-dimensional NMR. *Proceedings of the National Academy of Sciences of the United States of America* 86(15):5723-5727.
38. Puschendorf B, Petersen E, Wolf H, Werchau H, & Grunicke H (1971) Studies on the effect of distamycin A on the DNA dependent RNA polymerase system. *Biochem Biophys Res Commun* 43(3):617-624.
39. Mrksich M, Parks ME, & Dervan PB (1994) Hairpin Peptide Motif - a New Class of Oligopeptides for Sequence-Specific Recognition in the Minor-Groove of Double-Helical DNA. *Journal of the American Chemical Society* 116(18):7983-7988.
40. Wade WS, Mrksich M, & Dervan PB (1992) Design of Peptides That Bind in the Minor Groove of DNA at 5'-(a,T)G(a,T)C(a,T)-3' Sequences by a Dimeric Side-by-Side Motif. *Journal of the American Chemical Society* 114(23):8783-8794.
41. White S, Szewczyk JW, Turner JM, Baird EE, & Dervan PB (1998) Recognition of the four Watson-Crick base pairs in the DNA minor groove by synthetic ligands. *Nature* 391(6666):468-471.
42. Nickols NG, Jacobs CS, Farkas ME, & Dervan PB (2007) Improved nuclear localization of DNA-binding polyamides. *Nucleic acids research* 35(2):363-370.
43. Crowley KS*, et al.* (2003) Controlling the intracellular localization of fluorescent polyamide analogues in cultured cells. *Bioorganic & medicinal chemistry letters* 13(9):1565-1570.
44. Marini NJ*, et al.* (2003) DNA binding hairpin polyamides with antifungal activity. *Chemistry & biology* 10(7):635-644.
45. Olenyuk BZ*, et al.* (2004) Inhibition of vascular endothelial growth factor with a sequence-specific hypoxia response element antagonist. *Proceedings of the National Academy of Sciences of the United States of America* 101(48):16768-16773.

46. Nickols NG, Jacobs CS, Farkas ME, & Dervan PB (2007) Modulating hypoxia-inducible transcription by disrupting the HIF-1-DNA interface. *ACS chemical biology* 2(8):561-571.
47. Nickols NG & Dervan PB (2007) Suppression of androgen receptor-mediated gene expression by a sequence-specific DNA-binding polyamide. *Proceedings of the National Academy of Sciences of the United States of America* 104(25):10418-10423.
48. Muzikar KA, Meier JL, Gubler DA, Raskatov JA, & Dervan PB (2011) Expanding the repertoire of natural product-inspired ring pairs for molecular recognition of DNA. *Organic letters* 13(20):5612-5615.
49. Raskatov JA*, et al.* (2012) Modulation of NF-kappa B-dependent gene transcription using programmable DNA minor groove binders. *Proceedings of the National Academy of Sciences of the United States of America* 109(4):1023-1028.
50. Meier JL, Montgomery DC, & Dervan PB (2012) Enhancing the cellular uptake of Py-Im polyamides through next-generation aryl turns. *Nucleic acids research* 40(5):2345-2356.
51. Harki DA, Satyamurthy N, Stout DB, Phelps ME, & Dervan PB (2008) In vivo imaging of pyrrole-imidazole polyamides with positron emission tomography. *Proceedings of the National Academy of Sciences of the United States of America* 105(35):13039-13044.
52. Nagashima T*, et al.* (2009) Determination of pyrrole-imidazole polyamide in rat plasma by liquid chromatography-tandem mass spectrometry. *J Chromatogr B Analyt Technol Biomed Life Sci* 877(11-12):1070-1076.
53. Nagashima T*, et al.* (2009) Pharmacokinetic modeling and prediction of plasma pyrrole-imidazole polyamide concentration in rats using simultaneous urinary and biliary excretion data. *Biol Pharm Bull* 32(5):921-927.
54. Raskatov JA, Hargrove AE, So AY, & Dervan PB (2012) Pharmacokinetics of Py-Im Polyamides Depend on Architecture: Cyclic versus Linear. *Journal of the American Chemical Society* 134(18):7995-7999.
55. Synold TW*, et al.* (2012) Single-dose pharmacokinetic and toxicity analysis of pyrrole-imidazole polyamides in mice. *Cancer Chemother Pharmacol*.
56. Matsuda H*, et al.* (2011) Transcriptional inhibition of progressive renal disease by gene silencing pyrrole-imidazole polyamide targeting of the transforming growth factor-beta 1 promoter. *Kidney International* 79(1):46-56.
57. Raskatov JA*, et al.* (2012) Gene expression changes in a tumor xenograft by a pyrrole-imidazole polyamide. *Proceedings of the National Academy of Sciences of the United States of America* 109(40):16041-16045.
58. Yang F*, et al.* (2013) Antitumor activity of a pyrrole-imidazole polyamide. *Proceedings of the National Academy of Sciences of the United States of America* 110(5):1863-1868.

Chapter 2

Single-dose pharmacokinetic and toxicity analysis of pyrrole-imidazole polyamides in mice

The text of this chapter is taken from a manuscript coauthored with Timothy W. Synold[a], Bixin Xi[a], Jun Wu[a], Yun Yen[b], Benjamin C. Li[c], John W. Phillips[c], Nicholas G. Nickols[c], and Peter B. Dervan[c]

[a] *Department of Molecular Pharmacology, Beckman Research Institute of the City of Hope, Duarte, CA 91010*
[b] *City of Hope Medical Center, Duarte, CA 91010*
[c] *Department of Chemistry and Chemical Engineering, California Institute of Technology, Pasadena, CA 91125*

(Synold, T.W., Xi, B., Wu, J., Yen, Y., Li, B.C., Yang, F., Phillips, J.W., Nickols, N.G., Dervan, P.B. (2012) *Cancer Chemother. Pharmacol.*, **70**, 617-625)

Abstract

Pyrrole-Imidazole (Py-Im) polyamides are programmable, sequence specific DNA minor groove binding ligands. Previous work in cell culture has shown that various polyamides can be used to modulate the transcriptional programs of oncogenic transcription factors. In this study two hairpin polyamides with demonstrated activity against androgen receptor signaling in cell culture were administered to mice to characterize their pharmacokinetic properties. Py-Im polyamides were administered intravenously by tail vein injection. Plasma, urine, and fecal samples were collected over a 24hr period. Liver, kidney, and lung samples were collected postmortem. Concentrations of the administered polyamide in the plasma, excretion, and tissue samples were measured using LC/MS/MS. The biodistribution data were analyzed by both non-compartmental and compartmental pharmacokinetic models. Animal toxicity experiments were also performed by monitoring weight loss after a single subcutaneous (SC) injection of either polyamide. The biodistribution profiles of both compounds exhibited rapid localization to the liver, kidneys, and lungs upon injection. Plasma distribution of the two compounds showed distinct differences in the rate of clearance, the volume of distribution, and the AUCs. These two compounds also have markedly different toxicities after SC injection in mice. The variations in pharmacokinetics and toxicity *in vivo* stem from a minor chemical modification that is also correlated to differing potency in cell culture. The results obtained in this study could provide a structural basis for further improvement of polyamide activity both in cell culture and in animal models.

2.1 Introduction

The development of new DNA-targeted therapeutics is a promising frontier in the treatment of human disease. Py-Im polyamides are peptides of cyclic aromatic amino acids whose anti-parallel pairing confers sequence specific binding to the DNA minor groove [1-4]. Members of this class of compounds have been used to modulate gene expression programs in cell culture [5-13] and affect tumor growth in animal models [14-16].

Recently, a series of Py-Im polyamides have been developed to disrupt androgen receptor (AR) signaling [5, 6, 11], presenting an alternative strategy for therapeutic intervention in prostate cancer. These compounds were designed to bind to a 5'-WGWWCW-3' sequence contained within the consensus androgen response element (ARE) to prevent AR protein-DNA interactions. Cell culture experiments of LNCaP prostate cancer cells co-treated with dihydrotestosterone (DHT) and ARE-targeted polyamides have shown decreased expression of several AR driven genes such as *PSA, KLK2,* and *TMPRSS2* when compared to samples treated with DHT alone. Polyamide **1** inhibited DHT-induced genes in a dose dependent manner ranging from 0.74 μg/mL to 7.4 μg/mL, with 7.4 μg/mL being the most active concentration [11]. Polyamide **2** contains a minor structural modification where the (R)-2,4-diaminobutyric acid turn of **1** is replaced with an acetylated (R)-3,4-diaminobutyric acid. Due to this modification, polyamide **2** was found to have equivalent activity to **1** at 10 fold less concentration without significant changes to its DNA binding ability [6, 8, 11].

While the pharmacokinetics of other Py-Im polyamides have been published previously [17-20], the PK profiles of these structurally distinct ARE-targeted hairpin

polyamides have never been explored. For this study, mice were chosen as the preclinical model for the determination of polyamide concentrations in plasma, liver, kidney, and lung. In addition, urinary and fecal levels were measured to assess the relative importance of these routes of drug elimination. The data presented here represent the first detailed description of the *in vivo* pharmacokinetic and toxicological study of these molecules.

2.2 Materials and Methods

Chemicals and Reagents. Acetonitrile (ACN) and methanol (MeOH) were of HPLC-grade and purchased from Fisher Scientific (Fair Lawn, NJ, USA). Glacial acetic acid (ACS grade) was purchased from J.T. Baker (Phillipsburg, NJ, USA). Formic acid (99% pure) was from Acros organic (New Jersey, USA). Water was purified using the Millipore Milli-Q system (Milford, MA, USA). Mouse plasma for preparation of standards and quality controls (QC) were obtained from The City of Hope Medical Center Animal Center. Py-Im polyamides **1** - **4** were synthesized by solid phase synthesis as previously described [21, 22]. For structures of internal standards (INS) **3** and **4** see Fig. S2.1.

Animals for pharmacokinetic studies. Py-Im polyamide pharmacokinetic studies were performed in 10-12 week old female BALB/C mice (Charles River). Polyamides were solubilized in PBS (**1**) or PBS/DMSO (**2**) and administered via intravenous (IV) tail vein injection at concentrations of 7.5mg/kg and 5mg/kg, respectively. For each experiment, groups of 3 animals were euthanized at 0.083, 0.25, 0.5, 1, 2, 4, 8, and 24 hours after injection. Animals designated for the 4, 8, and 24 hour timepoints were housed in metabolic cages for collection of urine and feces as described below. All animal used in

the pharmacokinetic experiments were performed under an approved protocol at the City of Hope.

Animals for toxicology studies. Toxicities of polyamides **1** and **2** were measured after SC injections in 8-12 week old female C57BL/6 mice (Jackson Laboratory). In anticipation of future xenograft experiments, subcutaneous injection, which has been shown to be a viable route of polyamide delivery [20], was chosen as the desired delivery method. A single bolus of polyamide **1** or **2** in PBS/DMSO vehicle was given, and the animals were weighed daily and monitored closely for signs of duress for 7 days. Animals exhibiting >15% weight loss or signs of distress were euthanized according to regulations outlined by IACUC. Four animals were used in each group unless otherwise noted. This toxicology study was performed under an approved protocol at the California Institute of Technology.

Analytical methods development. Concentrations of polyamides **1** and **2** were analyzed by LC/MS/MS using a Waters Acquity UPLC system (Milford, MA, USA) interfaced with a Waters Quattro Premier XE Mass Spectrometer. HPLC separation was achieved using a Jupiter 4u Proteo 90A 150x2.0 mm column (Phenomenex, Torrance, CA, USA) proceeded by a Phenomenex C_8 guard column (Torrance, CA, USA). The column temperature was maintained at 30^{o}C. The mobile phase consisted of A (0.05% acetic acid in water) and B (0.05% acetic acid in acetonitrile). The following gradient program was used: 8% B (0-1 min, 0.3 ml/min), 16% B (3 min, 0.3 ml/min), 58% B (6 min, 0.3 ml/min), 90% B (7 min, 0.3 ml/min), 8% B (7.3 min, 0.3 ml/min). The total run time was 11.5 minutes. The auto-injector temperature was maintained at 5^{o}C. The strong needle wash solution was 5% formic acid in MeOH:ACN (2:8) for both compounds, and the

weak needle wash solution was 30% MeOH in water for compound **1** and 50% ACN in water for compound **2**. The electrospray ionization source of the mass spectrometer was operated in positive ion mode with a cone gas flow of 50 L/hr and a desolvation gas flow of 700 L/hr. The capillary voltage was set to 3.2 kV, and the cone and collision cell voltages were optimized to 32 V and 27 V for **1** and the INS **3**. Voltages were optimized to 31 V and 20 V for **2** and the INS **4**. The source temperature was 125^{o}C and the desolvation temperature was 470^{o}C. A solvent delay program was used from 0 to 4.0 minutes and from 6.1 to 11.5 minutes to minimize the mobile phase to flow to the source. MassLynx version 4.1 software was used for data acquisition and processing.

Positive electrospray ionization of all compounds produced abundant protonated molecular ions $(M+3H)^{3+}$. The fragmentations of these compounds were induced under collision induced dissociation condition. The precursor$\rightarrow$product ion combinations at m/z 453.52$\rightarrow$206.10 for **1**, 454.85$\rightarrow$210.24 for **3**, 467.45$\rightarrow$238.32 for **2**, and 469.9$\rightarrow$238.4 for **4** were used in multiple reaction monitoring (MRM) mode to determinate these compounds. The use of MRM provided sufficient specificity and sensitivity. MS/MS experimental conditions, such as collision energy and collision cell pressure, were optimized from continuous flow injection sample introduction of standard solutions. Under optimized assay conditions, the retention times for **1** and **3** were 5.0 min, and 5.5 min for **2** and **4**.

Plasma sample preparation. Plasma and urine samples were prepared for LC/MS/MS analysis by mixing 30 μL of plasma with 20 μL of 50% MeOH and 50% aqueous 1% HOAc. The mixture was vortexed and mixed with an additional 120 μL of 0.5% HOAc in MeOH:ACN (4:6) and 20 μL of 6.0 μg/mL INS in MeOH:1% aqueous HOAc (1:1).

The mixture was vortexed again for 2 minutes and centrifuged at the highest setting for 4 minutes. Next, 20 μL of the supernatant was transferred to a new tube and mixed with 180 μL of 50% MeOH:ACN (4:6) and 50% aqueous 1% HOAc.

Standard curves were prepared mixing untreated plasma with 20 μL of 50% MeOH and 50% aqueous 1% HOAc prepared with various concentrations of **1** and **2**. Internal standards were added as described above. The standard curves, as determined by linear regression, displayed good linearity ($r^2 > 0.99$) over the range tested for **1** (0.1 μg/mL to 30 μg/mL) and **2** (0.2 μg/mL to 20 μg/mL).

Urine and Fecal sample preparation. Urine and fecal samples were collected using metabolic cages (Ancare, Techniplast Metabolic Rack, 12 cages by Nalgene). Urine samples were collected at 3 time points over 24 hr and fecal samples were collected at 8 hr and 24 hr time points. Py-Im polyamides were extracted from urine according to the plasma extraction procedure described above.

Fecal samples were first dried at room temperature and then weighed and grounded to a powder. Approximately 100mg of powder was weighed out and reconstituted in distilled water (6 μL/mg powder). The fecal sample was then homogenized in a TissueLyser (Qiagen) for 2 minutes at 30Hz twice, and an additional 6 μL/mg of distilled water was added. Next, 30 μL of the fecal homogenate was mixed with 50 μL distilled water and 20μL of 50% MeOH and 50% aqueous 1% HOAc. The mixture was then vortex mixed with 0.1 mL 0.5% HOAc in MeOH:ACN (2:8) and 20 μL of 6.0 μg/mL INS in MeOH:1% aqueous HOAc (1:1) for 10 minutes and centrifuged at the highest setting for an additional 10 minutes. The supernatant was diluted with 50% MeOH:ACN (4:6) and 50% aqueous 1% HOAc.

Tissue sample preparation. Distribution of polyamides **1** and **2** was determined in the liver, kidneys, and lungs. The organs were harvested post-euthanasia and prepared via similar processes. A piece of the mouse organ was weighed and mixed with distilled water (3 μL/mg tissue). The tissue was then homogenized by pulsing three times on a TissueLyser for 2 minutes each at 30Hz. Next, 30 μL of the tissue homogenate was mixed with 20 μL of 50% MeOH and 50% aqueous 1% HOAc. The mixture was then vortex mixed with 0.12 mL 0.5% HOAc in MeOH:ACN (2:8) and 20 μL of 6.0 μg/mL INS in MeOH:1% aqueous HOAc (1:1) for 10 minutes and centrifuged at the highest setting for an additional 10 minutes. Samples treated with polyamide **1** were then diluted with 50% MeOH:ACN (4:6) and 50% aqueous 1% HOAc. Samples treated with polyamide **2** were diluted with 50% MeOH:ACN (4:6) and 50% aqueous 3% FA.

Pharmacokinetic Data Analysis. Plasma pharmacokinetic parameters were derived from polyamide concentration profiles using both non-compartmental and compartmental methods. Non-compartmental analysis was performed according to statistical moment theory and the rule of linear trapezoids, while compartmental analysis was performed in ADAPT II [24]. Pharmacokinetic parameters estimated from the non-compartmental analysis include the maximum concentration (C_{max}), the terminal elimination half-life ($t_{1/2}$), the mean residence time (MRT), the area under the concentration curve (AUC0-24h), the AUC extrapolated to infinity (AUC0-inf), and the clearance (CL). Additional plasma pharmacokinetic parameters determined from the compartmental analysis include the alpha and beta half-lives ($t_{1/2}$) and the apparent volume of distribution (V_d) Tissue pharmacokinetic parameters were determined non-compartmentally and included the

C_{max} and AUC0-24h. Urinary and fecal excretion data were expressed as the cumulative percentage of the administered dose.

pH Stability Analysis. The pH stability of Py-Im polyamides were analyzed as previously described [23]. In summary, 15 μL of a 10 μM solution of polyamide **1** or **2** in DMSO were incubated with 85 μL of buffer with pH of 2.5, 4, 7, or 10 (Fluka) at 37 ^{o}C for 24 hr. After incubation the sample were mixed with an equal volume of N,N-dimethylformamide and sonicated briefly. Next 20 μL of the sample solution was mixed with 180 μL of aqueous buffer containing 100 mM NH_4OAc and 25 μM methyl 4-nitro-1H-pyrrole-2-carboxylate as an internal standard. Analytical HPLC analysis was performed on a Beckman analytical HPLC.

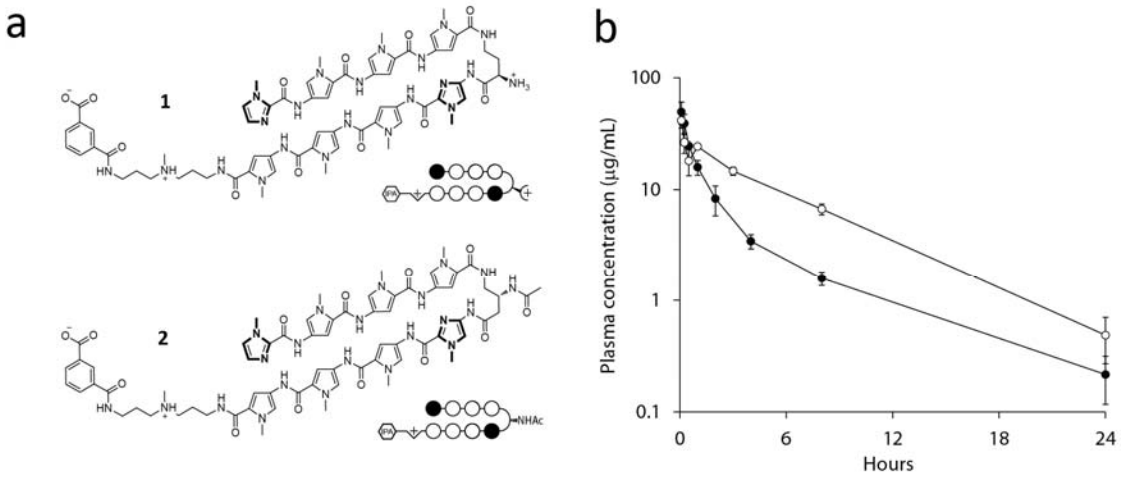

Fig. 2.1 (a) Chemical structures of polyamides **1** and **2**. **(b)** Plasma concentration versus time curves for **1** (closed circles) and **2** (open circles). Error bars indicate standard deviation.

2.3 Results

Plasma Distribution. The structures and plasma concentration profiles of polyamides **1** and **2** are shown in Fig. 2.1 and the pharmacokinetic parameters calculated non-compartmentally and using a 2-compartment model are summarized in Table 1. Plasma concentrations for both polyamides were well above the lower limit of quantification over

the entire time course. The average C_{max} was 49.4±11.2 μg/mL (mean±S.D., n=3) for **1** and 41.3±5.9 μg/mL for **2**. Both compounds exhibited a bi-exponential pattern of decay with first-order elimination, with initial and terminal $t_{1/2}$'s of 0.5 and 4.6 hours for **1**, and 0.1 and 4.2 hours for **2**. The average concentrations of **1** and **2** 24 hours post injection were 0.21±0.1 μg/mL and 0.49±0.2 μg/mL, respectively.

I. Non-compartmental analysis

Parameter	Compound	
	1	**2**
mg/kg	7.5	5
C_{max} (μg/mL)	49.4±11.2	41.3±5.9
Elimination $t_{1/2}$ (hr)	5.2	4.3
MRT (hr)	3.3	4.9
AUC_{0-t} (μg/mLxhr)	75.8	173.5
$AUC_{0-\infty}$ (μg/mLxhr)	77.4	176.5
CL (mL/hr)	1.8	0.6

II. Compartmental analysis

Parameter	Compound	
	1	**2**
mg/kg	7.5	5
C_{max} (μg/mL)	43.6	40.2
$t_{1/2}$ α (hr)	0.5	0.1
$t_{1/2}$ β (hr)	4.6	4.2
V_d (mL)	8.1	4
CL (mL/hr)	2.1	0.7
$AUC_{0-\infty}$ (μg/mLxhr)	67.5	144.8

Table 2.1 Plasma pharmacokinetic parameters of **1** and **2** after a single IV injection.

Despite using a higher dose, the AUC of **1** was 2-fold lower than **2** (67.5 versus 144.8 μg/mLxhr). Furthermore, the V_d of **1** was 2-fold higher than **2** (8.1 versus 4.0 mL). The calculated CL of **1** was 3-fold higher than **2** (2.1 versus 0.7 mL/hr).

Urine and Fecal Excretion. Concentration profiles of polyamides **1** and **2** in urine are shown in Fig. 2.2a. The urinary excretion of polyamide **1** was nearly complete by 4 hours, with a cumulative excretion of 5.7±2.9% of the administered dose. Urinary excretion of polyamide **2** was much more extensive and continued throughout the entire time course, with a cumulative urinary excretion at 24 hours of 46.0±15.2% of the administered dose.

Fecal recovery at 8 and 24 hours did not yield significant amounts of either polyamide, with cumulative recoveries after 24 hours of less than 5% of the administered dose (Fig. 2.2b). This finding is consistent with previously published results of a similarly sized polyamide [19].

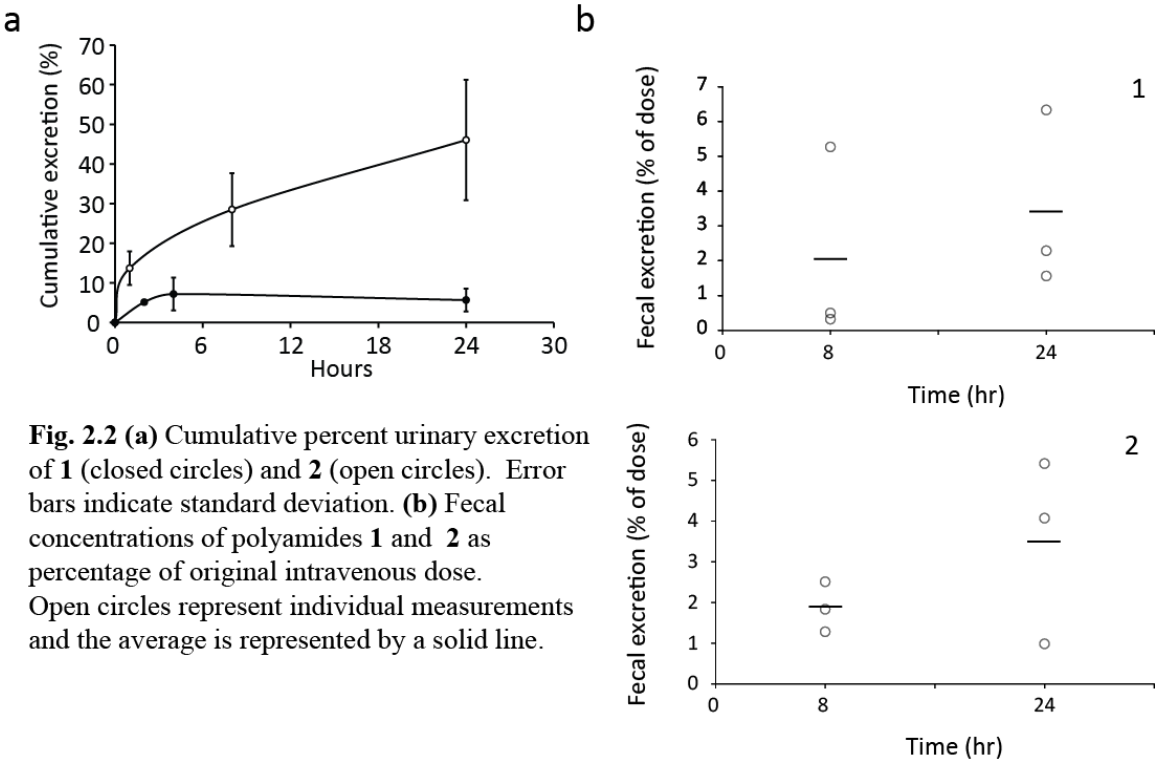

Fig. 2.2 (a) Cumulative percent urinary excretion of **1** (closed circles) and **2** (open circles). Error bars indicate standard deviation. **(b)** Fecal concentrations of polyamides **1** and **2** as percentage of original intravenous dose. Open circles represent individual measurements and the average is represented by a solid line.

Tissue Distribution. To examine tissue distribution, several organs previously reported to have polyamide localization were analyzed. Distribution profiles of polyamides **1** and **2** in the liver are shown in Fig. 2.3a. Both compounds localized rapidly to the liver post-administration. Polyamide **1** reached a maximum concentration of 11.7±1.3 μg/g at 5 minutes post injection. The concentration of polyamide **2** also peaked 5 minutes after injection at a maximum concentration of 43.8±0.7 μg/g. Both polyamides exhibited higher retention in the liver tissue than plasma. At the experiment endpoint 4.8±0.3 μg/g of **1** and 17.4±8.1 μg/g of **2** was found to remain in the liver. The AUC0-24h of polyamide **1** and **2** in the liver were 157.7 and 301.3 μg/gxhr, respectively. The localization of **1** and **2** to the liver is consistent with previously published positron emission tomography (PET) results of a related radiolabeled hairpin polyamide [23].

Polyamide pharmacokinetic profile in the kidneys is shown in Fig. 2.3b. Maximum kidney concentration of both polyamides was reached 5 minutes post injection with an average C_{max} of 27.0±2.9 μg/g and 35.1±2.8 μg/g for polyamides **1** and **2**, respectively. As in liver the rate of polyamide elimination from the kidney was slower than from the plasma, and the AUC0-24h of polyamides **1** and **2** in the kidney was 299.2 and 424.7 μg/gxhr, respectively. The increased concentrations of polyamide **2** relative to **1** in kidney were consistent with its higher rate of urinary excretion.

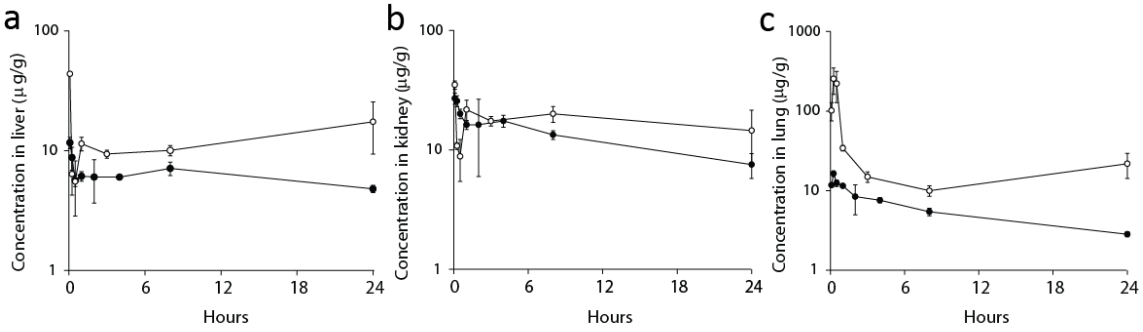

Fig. 2.3 Concentration versus time curves in **(a)** liver, **(b)** kidney, and **(c)** lung for **1** (closed circles) and **2** (open circles). Error bars indicate standard deviation.

Unlike liver and kidney, polyamide concentrations in the lung peaked at 15 minutes following injection for both compounds (Fig. 2.3c). The C_{max} of polyamide **2** in the lung was greater than 15 fold higher than compound **1,** with maximum concentrations of 256±93.1 μg/g for **2** and 16.4±1.4 μg/g for **1**. After an initial rapid decline, especially for polyamide **2**, concentrations in the lung were maintained above 2.8±0.2 μg/g and 21.8±7.6 μg/g for **1** and **2** respectively over the entire time course. The AUC0-24h of polyamide **1** and **2** in the lung were 130.6 and 523.5 μg/gxhr, respectively. Tissue PK parameters are summarized in Table 2.2.

Compound	1		2	
	C_{max} (μg/g)	AUC (μg/gxhr)	C_{max} (μg/g)	AUC (μg/gxhr)
Liver	11.7±1.3	157.7	43.8±0.7	301.3
Kidney	27.0±2.9	299.2	35.1±2.8	424.7
Lung	16.4±1.4	130.6	256±93.1	523.5

Table 2.2 Tissue pharmacokinetic parameters of **1** and **2** after a single IV injection.

Compound Stability. The stability of polyamides **1** and **2** at various physiological pHs were explored by incubating in pH 2.5, 4, 7, and 10 buffers at 37^{o}C for 24 hr. Analytical HPLC analysis of incubated samples did not display significant signs of degradation at any pH. See Online Resource Fig. S2.2.

Toxicity Study. Based on a defined threshold of greater than 15% weight loss over a 7 day observation period, the toxicity following a single subcutaneous injection of polyamide **1** or **2** was determined to be significantly different (Fig. 2.4). For polyamide **1**, critical weight loss occurred only at the highest dose level 10mg/kg. However, polyamide **2** demonstrated dose-limiting weight loss at both 4.5 mg/kg and 2.3 mg/kg. No additional signs of duress were observed in the animals treated with polyamide **1**, however, animals treated with polyamide **2** at doses of 4.5mg/kg and 2.3 mg/kg exhibited multiple signs of duress such as loss of ambulation and hunched posture in addition to weight loss.

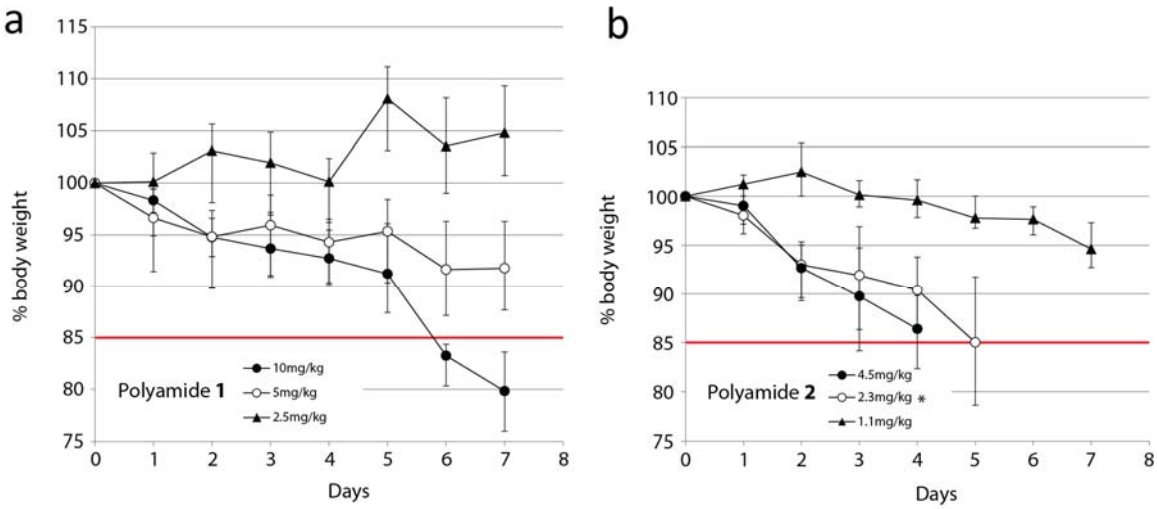

Fig. 2.4 Animal toxicity experiments for polyamide **(a) 1** and **(b) 2**. Animals were injected on day 0 and monitored for 7 days for weight loss and signs of duress. Error bars indicate standard deviation, n=4 (* n=3).

2.4 Discussion

Py-Im polyamides are sequence-specific DNA minor groove binders that have been shown to modulate gene expression regulated by transcription factors of oncological importance [10-13]. Of these compounds, two hairpin polyamides developed to disrupt AR signaling are of particular interest due to their gene regulation activities [6, 11] and potent cytotoxicity towards the LNCaP prostate cancer cell line [25]. While the two hairpin polyamides are structurally similar, a minor structural modification on the diaminobutyric acid turn was able to confer a ten-fold increase in the ability of polyamide **2** to downregulate *PSA* mRNA expression. In this study pharmacokinetic methods were employed to explore the differences in circulation, excretion, and tissue biodistribution of these ARE-targeted hairpin polyamides in mice.

Polyamide distribution in the plasma showed clearance profiles indicative of first-order elimination for both compounds (Fig. 2.1b and Table 2.1). This data is in line with published PK results of related polyamides in rats [17]. The maximum plasma concentration for polyamide **1** was found to be over 3 times the effect dosage for *PSA*

mRNA downregulation in cell culture, while the C_{max} for polyamide **2** was found to be approximately 29 times the effective concentration. Analysis of the plasma PK data showed that polyamide **2** exhibited a higher systemic exposure and lower clearance rate than polyamide **1**. Although the plasma clearance of polyamide **1** was ~3 fold faster than polyamide **2** it was not significantly eliminated through the urine or feces. Polyamide **2**, however, was largely eliminated through the urine (Fig. 2.2). The low amount of renal and biliary elimination of compound **1** may be suggestive of compound retention in the tissues or its metabolic degradation. A previous absorption, distribution, metabolism, excretion, and toxicity (ADMET) study had ascertained that polyamide **2** was resistant to liver microsomal degradation [5], however, the microsomal stability of polyamide **1** was never examined, and thus enzymatic degradation could be a route of elimination for this compound.

Interestingly, tissue analysis of the liver, kidneys, and lungs showed higher concentrations of polyamide **2** than **1** (Fig. 2.3 and Table 2.2). The three organs analyzed here have been previously documented as representative organs of polyamide localization [17,23], however, it is likely that the compounds were also taken up and retained in other tissues types, and that similar differences between the polyamides may exist in these sites. The differences in biodistribution between the two compounds may be attributable to differences in solubility. Polyamide **2** is less soluble than **1** in aqueous solutions and requires a polar aprotic cosolvent like DMSO for administration. Because the initial distribution of polyamide **2** to lung tissue was more than 15 fold higher than polyamide **1,** it is possible that compound **2** is precipitating out of solution as it reaches high local concentrations when passing through the lung immediately after an intravenous injection.

Alternatively, it is possible that polyamide **2** is preferentially taken up and retained by the lung tissue itself. This phenomenon has been previously described for many drugs and exogenous compounds, and the lungs have been demonstrated to have significant effects on the pharmacokinetics of drugs given intravenously [26]. Regardless of the mechanism of accumulation, once the concentration of polyamide **2** peaks in the lung, it apparently re-distributes unchanged back into circulation as indicated by a second peak in the plasma concentration versus time profile. Therefore, rather than being a site for drug elimination, the lung is serving as a reservoir for polyamide **2**, and merely delays its release back into the central compartment.

In addition to differences in biodistribution, animal toxicity studies also revealed major differences between the two compounds. Weight curve experiments following a single SC injection of **1** and **2** showed polyamide **2** to be more toxic (Fig. 2.4). Animals treated with **1** only showed significant weight loss at a dose of 10 mg/kg and no additional sign of duress was observed. In contrast, animals treated with polyamide **2** exhibited additional signs of physical duress in addition to weight loss at all concentrations except 1.1 mg/kg. Taken together, given its greater potency against the expression of select AR driven genes and its higher accumulation in normal tissues, the increased toxicity of polyamide **2** is likely due to off-target effects in normal organs. However, an alternative explanation for the increased toxicity seen with polyamide **2** could also be due to its relatively poor aqueous solubility. For example, in tissues where high local concentrations of polyamide **2** are achieved (i.e. lung), the compound may precipitate in capillaries, resulting in microinfarctions and ischemic tissue injury.

In conclusion, both polyamides **1** and **2** are bioavailable in mice after IV tail vein injection, and plasma concentration of both compounds are well above the levels required for gene regulation in cell culture. Although polyamide **2** exhibited more favorable plasma PK characteristics, with a higher AUC and slower clearance from plasma, it was found to be significantly more toxic to the animals. This study was the first to explore the PK properties of ARE-targeted hairpin polyamides, and it has revealed how a minor structural modification can influence the PK and toxicological properties of polyamides, thus setting the ground work for future xenograft experiments and providing a potential route to improve polyamide design for clinical applications.

References

1. Dervan PB, Edelson BS (2003) Recognition of the DNA minor groove by pyrrole-imidazole polyamides. Current Opinion in Structural Biology 13(3):284–299.

2. Hsu CF, Phillips JW, Trauger JW, Farkas ME, Belitsky JM, Heckel A, Olenyuk BZ, Puckett JW, Wang CCC, Dervan PB (2007) Completion of a programmable DNA-binding small molecule library. Tetrahedron 63(27):6146–6151.

3. Kielkopf CL, White S, Szewczyk JW, Turner JM, Baird EE, Dervan PB (1998) A structural basis for recognition of A·T and T·A base pairs in the minor groove of B-DNA. Science 282(5386):111–115.

4. White S, Szewczyk JW, Turner JM, Baird EE, Dervan PB (1998) Recognition of the four Watson-Crick base pairs in the DNA minor groove by synthetic ligands. Nature 391(6666):468–471.

5. Chenoweth DM, Harki DA, Phillips JW, Dose C, Dervan PB (2009) Cyclic pyrrole-imidazole polyamides targeted to the androgen response element. J Am Chem Soc 131(20):7182–7188.

6. Dose C, Farkas ME, Chenoweth DM, Dervan PB (2008) Next generation hairpin polyamides with (R)-3,4-diaminobutyric acid turn unit. J Am Chem Soc 130(21):6859–6866.

7. Matsuda H, Fukuda N, Ueno T, Tahira Y, Ayame H, Zhang W, Bando T, Sugiyama H, Saito S, Matsumoto K, Mugishima H, Serie K (2006) Development of gene silencing pyrrole-imidazole polyamide targeting the TGF-β1 promoter for treatment of progressive renal diseases. J Am Soc Nephrol 17:422–432.

8. Meier JL, Montgomery DC, Dervan PB (2012) Enhancing the cellular uptake of Py-Im polyamides throught next-generation of aryl turns. Nucleic Acids Res 40:2345–2356.

9. Muzikar KA, Nickols NG, Dervan PB (2009) Repression of DNA-binding dependent glucocorticoid receptor-mediated gene expression. Proc Natl Acad Sci U S A 106(39):16598–16603.

10. Nickols NG, Jacobs CS, Farkas ME, Dervan PB (2007) Modulating hypoxia-inducible transcription by disrupting the HIF-1-DNA interface. ACS Chem Biol 2(8):561–571.

11. Nickols NG, Dervan PB (2007) Suppression of androgen receptor-mediated gene expression by a sequence-specific DNA-binding polyamide. Proc Natl Acad Sci U S A 104(25):10418–10423.

12. Raskatov JA, Meier JL, Puckett JW, Yang F, Ramakrishnan P, Dervan PB (2012) Modulation of NF-kappaB-dependent gene transcription using programmable DNA minor groove binders. Proc Natl Acad Sci U S A 109(4):1023–1028.

13. Zhang Y, Sicot G, Cui X, Vogel M, Wuertzer CA, Lezon-Geyda KA, Wheeler JC, Harki DA, Muzikar KA, Stolper DA, Dervan PB, Perkins AS (2011) Targeting a DNA binding motif of the EVI1 protein by a pyrrole-imidazole polyamide. Biochemistry 50(48):10431–10441.

14. Dickinson LA, Burnett R, Melander C, Edelson BS, Arora PS, Dervan PB, Gottesfeld JM (2004) Arresting cancer proliferation by small-molecule gene regulation. Chem Biol 11:1583–1594.

15. Kashiwazaki G, Bando T, Yoshidome T, Masui S, Takagaki T, Hashiya K, Pandian GN, Yasuoka J, Akiyoshi K, Sugiyama H (2012) Synthesis and biological properties of highly sequence-specific-alkylating N-methylpyrrole-N-methylimidazole polyamide conjugates. J Med Chem 55:2057–2066.

16. Wang X, Nagase H, Watanabe T, Nobusue H, Suzuki T, Asami Y, Shinojima Y, Kawashima H, Takagi K, Mishra R, Igarashi J, Kimura M, Takayama T, Fukuda N, Sugiyama H (2010) Inhibition of MMP-9 transcription and suppression of tumor metastasis by pyrrole-imidazole polyamide. Cancer Sci. 101:759–766.

17. Fukasawa A, Aoyama T, Nagashima T, Fukuda N, Ueno T, Sugiyama H, Nagase H, Matsumoto Y (2009) Pharmacokinetics of pyrrole-imidazole polyamides after intravenous administration in rat. Biopharm Drug Dispos, 30(2):81–89.

18. Nagashima T, Aoyama T, Fukasawa A, Watabe S, Fukuda N, Ueno T, Sugiyama H, Nagase H, Matsumoto Y (2009) Determination of pyrrole-imidazole polyamide in rat plasma by liquid chromatography-tandem mass spectrometry. J Chromatogr B Analyt Technol Biomed Life Sci 877(11-12):1070–1076.

19. Nagashima T, Aoyama T, Yokoe T, Fukasawa A, Fukuda N, Ueno T, Sugiyama H, Nagase H, Matsumoto Y (2009) Pharmacokinetic modeling and prediction of plasma pyrrole-imidazole polyamide concentration in rats using simultaneous urinary and biliary excretion data. Biol Pharm Bull 32(5):921-927.

20. Raskatov JA, Hargrove AE, So AY, Dervan PB (2012) Pharmacokinetics of Py-Im polyamides depend on architecture: cyclic versus linear. J Am Chem Soc Accepted.

21. Belitsky JM, Nguyen DH, Wurtz NR, Dervan PB (2002) Solid-phase synthesis of DNA binding polyamides on oxime resin. Bioorg Med Chem 10(8):2767-2774.

22. Nickols NG, Jacobs CS, Farkas ME, Dervan PB (2007) Improved nuclear localization of DNA-binding polyamides. Nucleic Acids Res 35(2):363-370.

23. Harki DA, Satyamurthy N, Stout DB, Phelps ME, Dervan PB (2008) In vivo imaging of pyrrole-imidazole polyamides with positron emission tomography. Proc Natl Acad Sci U S A 105(35):13039-13044.

24. D'Argenio DZ, Schumitzky AX, Wang X (2009) ADAPT 5 User's Guide: Pharmacokinetic/Pharmacodynamic Systems Analysis Software. Biomedical Simulations Resource, Los Angeles.

25. Jacobs CS, Dervan PB (2009) Modifications at the C-terminus to improve pyrrole-imidazole polyamide activity in cell culture. J Med Chem 52:7380–7388.

26. Boer F (2003) Drug handling by the lungs. Br J Anaesth 91(1):50-60.

2.5 Supplemental Material

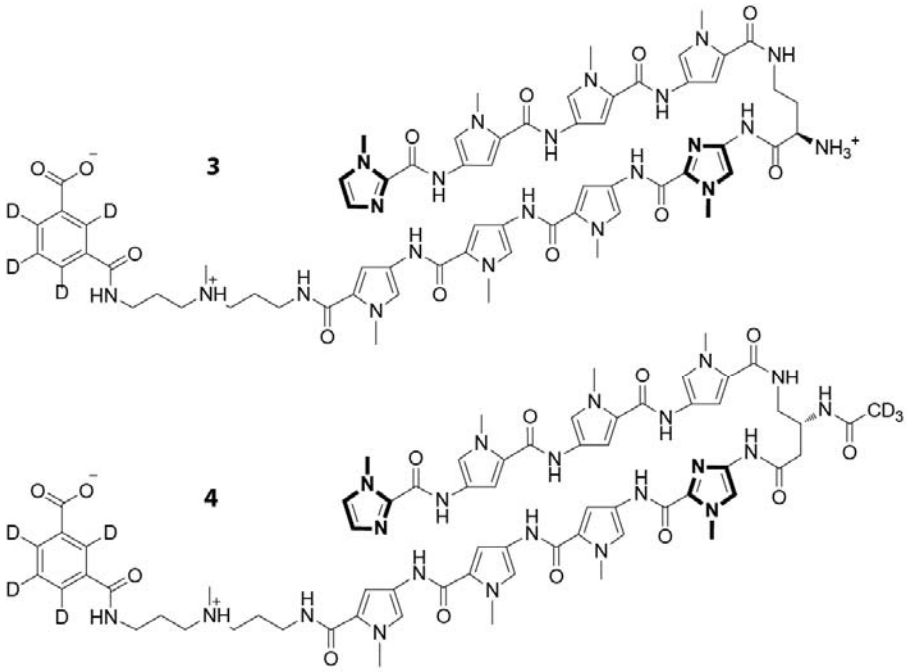

Fig. S2.1. Chemical structures of standards **3** and **4** used in LC/MS/MS analysis. Polyamide **3** was used asthe internal standard for **1**, and polyamide **4** was used as the standard for **2.**

Chapter 3

Antitumor activity of a pyrrole-imidazole polyamide

The text of this chapter is taken from a manuscript coauthored with Nicholas G. Nickols[a,b], Benjamin C. Li[a], Georgi K. Marinov[c], Jonathan W. Said[d], and Peter B. Dervan[a]

[a] *Division of Chemistry and Chemical Engineering, California Institute of Technology, Pasadena, CA*

[b] *Department of Radiation Oncology, David Geffen School of Medicine at UCLA, Los Angeles, CA*

[c] *Division of Biology, California Institute of Technology, Pasadena, CA*

[d] *Department of Pathology and Laboratory Medicine, David Geffen School of Medicine at UCLA, Los Angeles, CA*

(Yang, F., Nickols, N.G., Li, B.C., Marinov, G. K., Said, J. W., Dervan, P.B. (2013) *Proc. Natl. Acad. Sci.*, **110**, 1863-1868)

Abstract

Many cancer therapeutics target DNA and exert cytotoxicity through the induction of apoptosis by DNA damage and inhibition of transcription. We report that a DNA minor groove binding hairpin pyrrole-imidazole (Py-Im) polyamide interferes with RNA polymerase II (RNAP2) activity in cell culture. Polyamide treatment activates p53 signaling in LNCaP prostate cancer cells without detectable DNA damage. Genome-wide mapping of RNAP2 binding shows reduction of occupancy preferentially at transcription start sites (TSS), while occupancy at enhancer sites are unchanged. Polyamide treatment results in a time- and dose-dependent depletion of RNAP2 large subunit RPB1 that is preventable with proteasome inhibition. This polyamide demonstrates antitumor activity in a prostate tumor xenograft model with limited host toxicity.

3.1 Introduction

Several chemotherapeutics including the anthracyclines and cisplatin exert part of their cytotoxicity through the inhibition of transcription (1). Transformed cells often require constant expression of anti-apoptotic genes for survival, making transcription inhibition a relevant therapeutic strategy in oncology (1, 2). Many radio- and chemotherapy treatments that target DNA, including UV irradiation, cisplatin, and the topoisomerase inhibitors, introduce obstacles to RNAP2 elongation by generating bulky or helix distorting lesions (3-5). In cell culture experiments, transcription blockade has been shown to induce the degradation of the RNAP2 large subunit (RPB1), and function as a signal for p53 mediated apoptosis (6, 7). While many DNA targeted therapeutics effectively inhibit transcription and induce apoptosis, clinical treatment with genotoxic agents can also damage DNA in normal cells, increasing symptomatic toxicity and potentially leading to secondary cancers (8). The question arises whether high affinity, non-covalent DNA-binding ligands offer an approach to transcription inhibition without DNA damage.

Hairpin Py-Im polyamides are synthetic oligomers with programmable sequence recognition that bind the minor groove of DNA with high affinity (9). Py-Im polyamide-DNA binding induces allosteric changes in the DNA helix that can interfere with protein-DNA interactions (10, 11). Py-Im polyamides have been used as molecular probes in cell culture to modulate inducible gene expression pathways (12-14). In rodents, 8-ring hairpin Py-Im polyamides circulate in blood for several hours after administration, and affect changes in gene expression in tissues (15-17).

We have previously reported that polyamide **1** (Fig. 3.1), which targets the sequence 5'-WGWWCW-3' found in the androgen response element, inhibited a subset of dihydrotestosterone (DHT) induced genes in LNCaP cells (12). In this paper we explore the effects of this polyamide on the RNAP2 transcription machinery. We find that RNAP2 is preferentially reduced from transcription start sites genome-wide without significant perturbation at enhancer loci. This is accompanied by proteasome dependent degradation of the RNAP2 large subunit RPB1. Polyamide treatment induces p53 accumulation that is consistent with what is observed for other transcription inhibitors that interact with DNA (4, 5), but without evidence of DNA damage. This polyamide demonstrates efficacy *in vivo* against prostate cancer xenografts in mice with limited host toxicity.

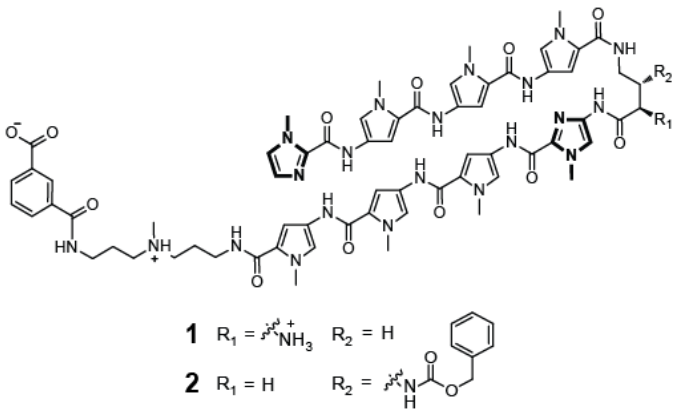

Fig. 3.1. Structure of polyamide **1** and **2**.

3.2 Materials and Methods

Compounds and reagents. Py-Im polyamides **1**, **2** and **3** were synthesized on oxime resin as described (18-20). (R)-MG132 (MG132) was from Santa Cruz Biotechnology.

Cell viability assays. LNCaP cells were plated in clear bottom 96 well plates at 5,000-7,500 cells per well. The cells were allowed to adhere for 24-36h before compounds were added in fresh media. Cell viability was determined by the WST-1 assay (Roche)

for **1** and **2** after 24 h or 72 h incubation with cells. Cells in cytotoxicity rescue experiments were treated with **2** alone or with 3μM for 24h. For cell cycle arrest experiments LNCaP cells were seeded at 2,500-5,000 cells per well in normal media and allowed to adhere for 24-36h. The media was replaced with media supplemented with 0.5% FBS and incubated for 48h prior to treatment with compound.

***In vivo* xenografts experiments**. All mice experiments were conducted under an approved protocol by the Institutional Animal Care and Use Committee of the California Institute of Technology. Male NOD scid gamma (NSG) mice were purchased from The Jackson Laboratory. The animals were individually caged and maintained on a standard light-dark cycle. NSG mice were engrafted with LNCaP cells (2.5 million cells) in a mixture of 1:1 media and matrigel in the left flank. Tumors were grown to ~100mm^3 (LxW^2) before beginning treatment with compound or vehicle. Py-Im polyamide **1** was administered once every 3 days in a 5% DMSO:PBS vehicle solution until the experiment endpoint.

Serum measurements. To investigate if polyamide **1** could be detected in peripheral blood after SC injections, 120nmol of **1** (in 5% DMSO/PBS) was injected into the right flank of four C57BL/6 mice. Blood was collected from anesthetized mice via retroorbital collection at 5 minutes, 4 h, and 12 h after injection, then processed by methods previously described and analyzed by HPLC (21). For measurement of serum PSA (KLK3) and uric acid, blood was collected from anesthetized mice via retroorbital collection at experimental endpoint and serum was separated from blood by centrifugation. Serum PSA (KLK3) was measured by ELISA (R&D systems) according to manufacturer's instructions. Uric acid was measured as described (22).

Chromatin immunoprecipitation. Genomic occupancy of RNA polymerase II was determined by chromatin immunoprecipitation (ChIP) with the 4H8 antibody (Abcam). LNCaP cells were plated at 35 million cells per plate in RPMI supplemented with 10% CTFBS and allowed to adhere for 24-36 h. The cells were treated with compound **1** in fresh media (10% CTFBS) for 48h. Cells treated and untreated with **1** were incubated with 1nM DHT for 6h. Two step crosslinking was performed as previously described (23). After DSG removal, chromatin was immunopreciated by previously published methods (24). DNA was harvested by phenol chloroform extraction and purified with the QIAquick purification kit (Qiagen). Quantitative PCR was used to validate enrichment at the GAPDH transcription start site (Primers: F- GGTTTCTCTCCGCCCGTCTT , R-TGTTCGACAGTCAGCCGCAT) compared to an internal negative locus (Primers: F-TAGAAGGGGGATAGGGGAAC, R-CCAGAAAACTGGCTCCTTCTT). Each sample was immunoprecipated as 5 technical replicates. The 3 most consistent samples were combined and submitted for sequencing on an Illumina genome analyzer. Biological replicates were acquired.

Data processing and analysis. Sequencing reads were trimmed down to 36bp and then mapped against the male set of human chromosomes (excluding all random chromosomes and haplotypes) using the hg19 version of the human genome as a reference. Bowtie 0.12.7 was used for aligning reads (25), with the following settings: "-v 2 -t --best --strata". Signal profiles over genomic locations were generated using custom written python scripts; the refSeq annotation was used for gene coordinates. Enhancers and promoters were defined using previously published histone marker data (26). ChIP-seq peaks were called using MACS2 with default settings (27). Enhancers were defined as H3K4me1-positive regions that did not intersect with H3K4me3-positive regions and promoters as H3K4me3-positive regions that did not intersect with H3K4me1-positive

regions. Clustering was performed with Cluster 3.0 (28) and visualized with Java TreeView (29).

Comet Assay. LNCaP cells were plated at 1million cells per 10cm plate and allowed to adhere for 24 to 36h. Cells were then incubated with either 10μM **1** for 48h or 5μM doxorubicin for 4h. DNA damage was assayed using the Trevigen CometAssay® system and samples were prepared from harvested cells according to the manufacture protocol. Comets were imaged on a confocal microscope (Exciter, Zeiss) at 10x magnification. Percentage of DNA in the tail was determined using Comet Assay Lite IV (Perceptive Instruments). More than one hundred comets were scored for each condition.

Immunoblot assay. Samples for immunoblot analysis were prepared by plating LNCaP or DU145 cells at 1million cells per 10 cm plate. Cells were allowed to adhere for 24-36hr prior to incubation with compound. After the appropriate incubation time cells were washed once with ice cold PBS and harvested in ice cold 125μL lysis buffer (50mM Tris-HCl pH 7.4, 150mM NaCl, 1mM EDTA, 1% Triton X100) containing protease inhibitor cocktail (Roche), 1mM PMSF (Sigma), and phosphatase inhibitors (Sigma). Samples were allowed incubate on ice for 10min with vortexing once every 3min. Cellular debris was pelleted by spinning at 14,000rpm for 15min to collect the supernatant. Samples were then quantified for protein content with the Bradford assay (Bio-rad) and boiled with 4x sample buffer (Li-Cor) for 5min. Protein electrophoresis was performed in 4-20% precast Tris glycine SDS gels (Bio-rad) and transferred to PVDF membranes. Membrane blocking was done with Odyssey Blocking Buffer (Li-Cor). The following antibodies used to probe changes in protein levels or phosphorylation states: RBP1 (Santa Cruz Biotechnology, N20), p53 (Santa Cruz Biotechnology, DO1), phospho-Chk2-Thr68

(Cell Signaling Technology), Phospho-p53-Ser15 (Cell Signaling Technology), phosphor-H2A.X-Ser139 (Cell Signaling Technology), phosphor-ATM-Ser1981 (Abcam), phosphor-DNA-PKcs-Ser2056 (Abcam), and β-actin (Abcam). Near-IR secondary antibodies (Li-Cor) were used for imaging. Experiments were performed in biological replicates.

Flow cytometry. To determine cell cycle distribution of LNCaP cells grown in normal media or under serum starved conditions 1million cells were seeded to each 10cm plate and allowed to adhere for 24 -36h. Media was then replaced with fresh normal media (10% FBS) or serum starved media (0.5% FBS) and incubated for an additional 48h. Cells were then trypsinized and prepared for analysis as previously described (30). Samples were analyzed in biological triplicate on a FACSCalibur (Becton-Dickinson) instrument. Data analysis was performed using FlowJo 7.6.5.

Quantitative RT-PCR. RNA was extracted using RNEasy columns (Qiagen) according to manufacturer's protocols. cDNA was generated from RNA by reverse transcriptase (Transcriptor First Strand cDNA kit, Roche). Quantitative real-time RT–PCR was performed using SYBR Green PCR Master Mix (Applied Biosystems) on an ABI 7300 instrument. mRNA was measured relative to ß glucuronidase as an endogenous control. For primer sequences see **Table S3.1.**

Confocal microscopy. Cells were plated in 35mm optical dishes (MatTek) and dosed with polyamide **3** at 2μM for 24 h with or without 3μM MG132. Cells were then washed with PBS and imaged on a confocal microscope (Exciter, Zeiss) using a 63x oil immersion lens. Confocal imaging was performed following established protocols (18).

Histology and immunohistochemistry. Tumors were resected immediately after

euthanasia and fixed in neutral buffered formalin. Selected samples were embedded in paraffin, sectioned and stained with hematoxylin and eosin (H&E). Selected sections were assessed by deoxynucleotidyltransferase dUTP nick-end labeling (TUNEL) as described (31).

Thermal denaturation assays. Polyamides **1** and **2** were incubated with duplex DNA 5'-CGATGTTCAAGC-3', which contains the predicted target site for these compounds (underscore). Melting temperature analyses were performed on a Varian Cary 100 spectrophotometer as described (32). Melting temperatures were defined as a maximum of the first derivative of absorbance at 260 nm over the range of temperatures.

Statistical analysis. Statistical significance was calculated using the student's t test with two tailed variance. Results were considered significant when $p < 0.05$.

3.3 Results

The effects of polyamide 1 on global occupancy of RNAP2. Polyamide **1** was previously shown to inhibit the induction of a subset of DHT driven genes in LNCaP cell culture (12). We interrogated the effects of **1** on the RNAP2 transcription machinery by mapping the global occupancy of RNAP2 using ChIP-seq. Under DHT induction, select androgen receptor (AR) driven genes, such as *KLK3*, showed increased RNAP2 occupancy over genic regions, which was decreased in the presence of **1** (Fig. 3.2A). While RNAP2 occupancy across constitutively expressed genes such as *GAPDH* did not change with DHT induction, cotreatment with **1** reduced RNAP2 occupancy across these genes (Fig. 3.2B). This reduction in RNAP2 occupancy by **1** was in the context of a global decrease of RNAP2 occupancy across genic regions (Fig. S3.1), particularly at transcription start sites (TSS) (Fig. 3.2C). However, **1** did not significantly change

RNAP2 occupancy at enhancer loci (Fig. 3.2D), suggesting **1** may affect the active elongation of RNAP2 without disturbing the transcription apparatus anchored at enhancers, and that the observed differences in RNAP2 occupancy are not due to technical variation in ChIP success between experiments. Reduction in DNA occupancy of RNAP2 has also been reported in cells treated with α-amanitin, a cyclic octapeptide inhibitor of RPB1 (33).

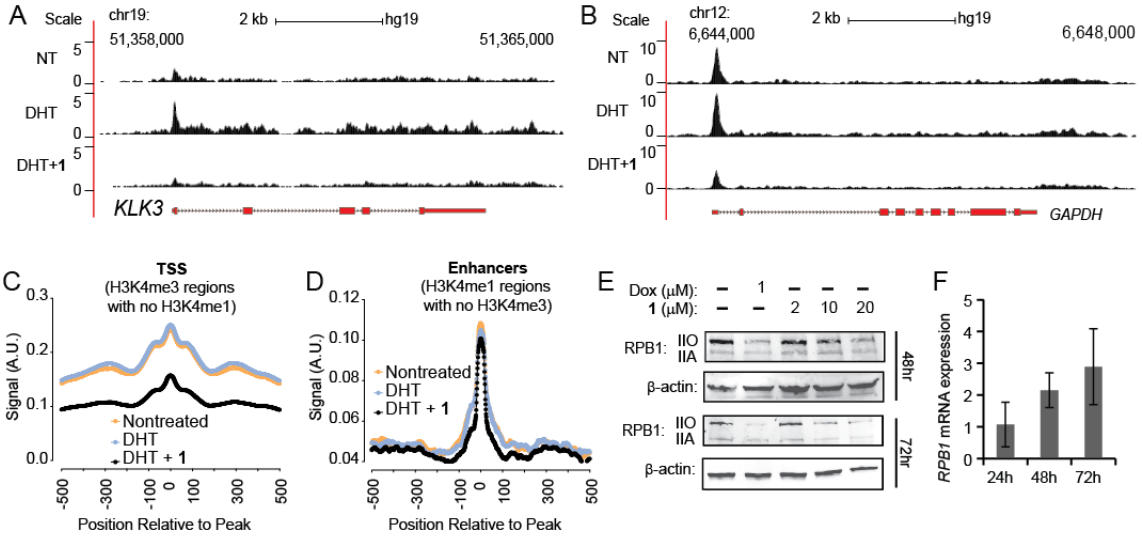

Fig. 3.2. Global effects on RNAP2. Genome browser tracks of RPB1 occupancy from untreated, DHT treated, DHT + **1** treated samples over **(A)** an AR driven gene, *KLK3* (*PSA*), and **(B)** a housekeeping gene, GAPDH. **(C)** Genomic RNAP2 occupancy at transcription start sites show comparable levels of enrichment for nontreated and DHT treated samples. Samples treated with DHT + **1** exhibited much lower occupancy. **(D)** Genomic RNAP2 occupancy at enhancer regions is largely unchanged between the three treatment conditions. **(E)** Immunoblot of RPB1 protein in LNCaP cells treated with 1μM doxorubicin (dox) for 16h, or **1** at 2μM, 10μM, and 20μM for 48 and 72h. **(F)** Quantitative RT-PCR measurement of RPB1 transcript levels after LNCaP cells are treated with 10μM **1** for the indicated times. Relative expression is normalized against nontreated cells. Data represent mean±s.d. of biological quadruplicates.

Inhibition of RNAP2 elongation can be caused by a multitude of genotoxic agents and often results in the degradation of the RPB1 subunit (3, 34, 35). Indeed, in addition to reduced RNAP2 DNA occupancy, immunoblot analysis of LNCaP cells treated with **1** shows depletion of RPB1 in a time- and concentration-dependent manner (Fig. 2E). To examine if the effects of RPB1 degradation was transcription dependent we measured

levels of RPB1 mRNA (Fig. 2F). The expression of RPB1 modestly increased with polyamide treatment, suggesting this depletion is post-transcriptional.

Polyamide cytotoxicity is reduced by proteasomal inhibition and serum starvation. Inhibition of RNAP2 has been reported to induce apoptosis (4, 6, 36), and may contribute to polyamide cytotoxicity observed in LNCaP cells cultured with **1** (Fig. 3.3A). A previous study with trabectidin, a DNA minor groove alkylator that causes RPB1 degradation, showed the toxicity induced by the molecule can be reduced by cotreatment with the proteasome inhibitor MG132(36). To evaluate if polyamide-induced toxicity was also reducible by proteasomal inhibition we treated LNCaP cells with **2** in the presence and absence of MG132. We developed analog **2** specifically for this application because prolonged incubation with MG132 alone is cytotoxic, and conjugation of an aryl group to the γ-aminobutyric acid turn have been shown to improve cellular uptake and cytotoxicity of polyamides. Cell viability experiments showed that **2** induced cell death more rapidly than **1** without significant change to DNA binding (Fig. S3.2A-B). Cell culture experiments revealed coincubation with MG132 reduced cytotoxicity induced by **2** (Fig. 3.3B) and prevented degradation of RPB1 (Fig. 3.3C). Polyamide nuclear uptake was not affected by MG132 (Fig. S3.2C-D). In addition, cytotoxicity studies of cells treated with UV radiation and α–amanitin have shown increased cellular sensitivity to transcription inhibition upon S phase entry(6, 37). Similarly, **2** was less toxic to LNCaP cells arrested in G_1/G_0 by serum starvation as compared to cells grown in normal media (Fig. 3.3D and S3.2E).

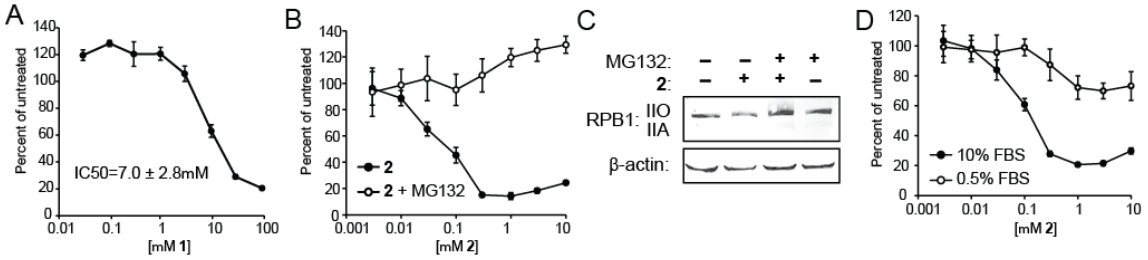

Fig. 3. 3. (A) Cytotoxicity of 1 in LNCaP cells after incubation with **1** for 72h. Data represent mean ± s.d. IC50 is calculated from 3 independent experiments and the error is a 95% confidence intervals. **(B)** Cell viability at 24h of LNCaP cells treated with varying concentrations **2** with and without proteasome inhibitor MG132 (3μM, 24h); proteasome inhibition reduces cytotoxicity of **2**. **(C)** Immunoblot of RPB1 protein in LNCaP cells treated with 10μM **2** for 12h followed by 10 μM MG132 for 4h. **(D)** Cytotoxicity of **2** in LNCaP cells incubated with 10% FBS or with 0.5% FBS for 24h. Serum starvation decreases percent of cells in the S phase from 8.5% to 4.4% (SI Fig. 2). Data represent mean of biological triplicates and error bars represent s.d.

Accumulation of p53 and expression of p53 targets in the absence of DNA damage. Previously published microarray data of LNCaP cells cotreated with DHT and **1** revealed the induction of several p53 target genes (12). Despite depletion of RPB1, treatment of LNCaP cells with **1** alone induced expression of p53 genes that are characteristic of genotoxic stress (Fig. 3.4A) (38). Many of these genes were previously observed to be induced in A549 cells treated with polyamide as well as polyamide-alkylator conjugates (14, 39). To examine if direct DNA damage was contributing to p53 activity, we looked for evidence of DNA damage in LNCaP cells after extended treatment with **1**. Alkaline comet assay showed no evidence of DNA fragmentation (Fig. 3.4B). Additionally, treatment with **1** did not induce cellular markers of DNA damage including phosphorylation of γH2A.X, ATM, DNA-PKcs, p53, or Chk2 (Fig. 3.4C). However, modest accumulation of p53 and PARP cleavage were observed. This data suggest that **1** activates p53 through transcriptional inhibition without DNA damage, a mechanism that has been observed for non-DNA targeting agents that exert transcriptional stress such as the protein kinase inhibitor 5,6-dichlorobenzimidazole (DRB) and α-amanitin(5, 6, 40).

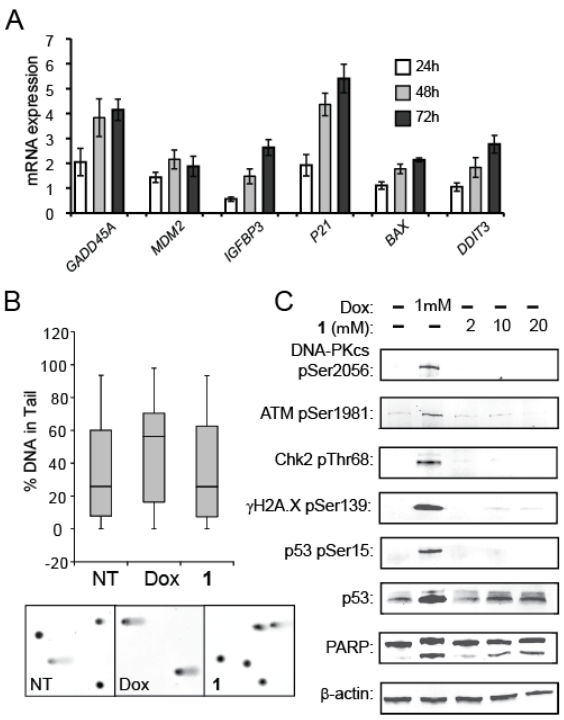

Fig. 3.4. (A) Induction of p53 target genes (*GADD45A, MDM2, IGFBP3, P21, BAX*) and DNA damage inducible transcript 3 (*DDIT3*), by **1** (10μM) at 24h, 48h, and 72h. Data represent the mean of 4 biological replicates and error bars represent s.d. **(B)** Alkaline comet assay of LNCaP cells treated with vehicle, dox (5μM, 4h), **1** (10μM, 48h). Error bars represents max and min, boxes represents the upper and lower quartiles and median. Representative comets for each treatment are shown. Effects of **1** are indistinguishable from the non-treated control, while dox treatment significantly increases comet-tail percent of DNA. p=0.00043. **(C)** DNA damage markers after treatment of LNCaP cells with **1**. There is no evidence of phosphorylated DNA-PKcs, ATM, Chk2, p53 or γH2A.X. Accumulation p53 and PARP cleavage are observed. Data is representative of biological triplicates

Effects of polyamide treatment on prostate cancer xenografts. We recently reported the toxicity and pharmacokinetic (PK) profile of **1** in mice (16). Subcutaneous (SC) injection of **1** also results in detectable circulation (Fig. S3.3). We thus selected this molecule for further testing against xenografts *in vivo*. Male NSG mice bearing LNCaP xenografts were treated with either vehicle or 20nmol (~1 mg/kg) **1** by SC injection once every 3 days for a cycle of three injections. At the experimental end point, mice treated with **1** had smaller tumors and lower serum PSA as compared to vehicle controls (Fig. 3.5A-B). Immunohistological analysis of selected tumors showed evidence of cell death by TUNEL stain (Fig. 3.5C). While tumor-free NSG mice treated with **1** under this regimen showed no signs of distress or weight loss, LNCaP tumor-bearing NSG mice exhibited weight loss by the experimental end point (Fig. S3.4). This was accompanied by an elevation in serum uric acid that was not observed in either control group (Fig. 3.5D).

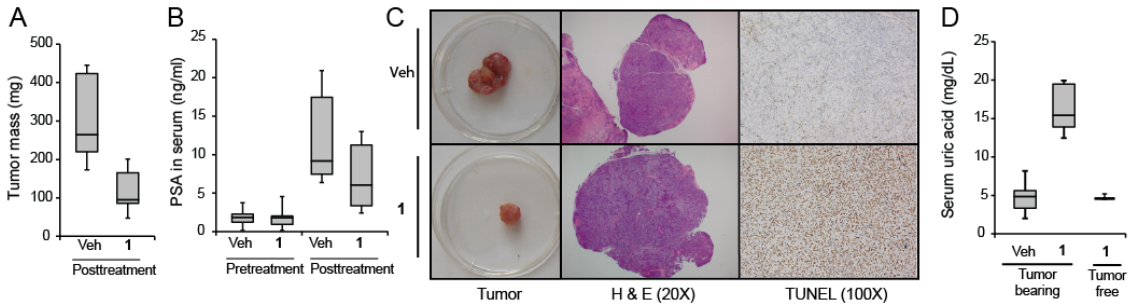

Fig. 3.5. Polyamide **1** demonstrates antitumor activity in prostate cancer xenografts. **(A)** Male immuno-compromised mice were engrafted with LNCaP cells and observed until tumors reached ~100mm3. Tumor bearing mice were then treated with 20nmol **1** (n=12) or vehicle (n=13) by SC injections into the flank distal to the tumor once every three days for a total of three injections. Mice were euthanized and tumors resected and weighed two days after the final injection. Tumors from mice treated with **1** were smaller (mean: 112mg, median: 94mg, range: 47-201mg) than those of vehicle treated mice (mean:310mg, median: 292mg, range: 173-440mg). Error bars represents max and min, boxes represents the upper and lower quartiles and median. p=1.6E-5. **(B)** Serum PSA measured by ELISA pre- and post- treatment. Serum PSA is lower in the post-treatment serum of mice treated with **1** as compared to vehicle. p=0.024. **(C)** Selected tumors and histological stains of tumor cross-sections from mice treated with vehicle or **1**. **(D)** Treatment of LNCaP tumor bearing mice with **1** increases serum uric acid as compared to vehicle controls and polyamide treated, non-tumor bearing mice. p=3.2E-9.

3.4 Discussion

DNA targeting agents including cisplatin, the anthracyclines, minor groove binders and UV radiation have been demonstrated to affect a multitude of DNA dependent enzymes such as the RNA polymerases, DNA polymerase, topoisomerases, and helicases (21, 27, 28). Our research group and others have used polyamides as molecular tools to modulate gene expression programs (12-14, 29). The programmable sequence specificity of Py-Im polyamides offers a unique mechanism to target specific transcription factor – DNA interfaces and thereby modulate particular gene expression pathways. In previous studies we've focused our analysis on specific changes to inducible pathways of gene expression. For example, we have shown polyamide **1** affects approximately 30% of the DHT-induced transcripts in LNCaP cells, which may result from inhibition of the transcription factor AR-DNA interface (12). However, the cellular cytotoxicity of this polyamide may not be due to only inhibition of DHT-induced gene expression since analogs of **1** exhibits toxicity in a variety of cancer cells (19). It is more

likely that polyamides perturb a multitude of DNA dependent cellular processes (transcription, replication) that contribute to cytotoxicity. In this study we show that **1** interferes with RNAP2 elongation resulting in the degradation of RPB1, activation of p53, and triggering of apoptosis, without detectable genomic damage.

Our previous study has shown polyamide **1** decreased the expression of a large number of genes in LNCaP cells (12). To examine the effect of **1** on the transcription machinery we performed genome-wide mapping of RNAP2 occupancy by ChIP-seq. We found that while DHT induction increased RNAP2 occupancy at select AR driven genes, cotreatment with **1** caused a genome-wide decrease of RNAP2 occupancy across genic regions. The effect was most pronounced at transcription start sites. Interestingly, RNAP2 occupancy at enhancer loci, where the transcription assemblies may be attached to via contacts through other proteins, was not significantly affected by polyamide treatment. This suggests polyamide **1** may preferentially affect RNAP2 loading at regions where RNAP2 is actively engaged, a mechanism that has been previously proposed for the gene regulatory activity of polyamides (41).

The displacement of RNAP2 from DNA is caused by many DNA damaging agents that pose an impediment to RNAP2 elongation, this effect is normally coupled with the degradation of large RNAP2 subunit RPB1. Indeed, the cellular level of RPB1 in LNCaP cells was found to decrease in both a time- and concentration-dependent manner when treated with polyamide **1**. Polyamide **2**, a more cytotoxic analog of **1**, also reduced cellular RPB1 in LNCaP cells and induced cell death. Cotreatment of **2** with a proteasomal inhibitor MG132 was able to prevent the degradation of RPB1 and reduce the toxicity of **2** in cell culture. In addition, the cytotoxic effects of other RNAP2

inhibitors were found to be attenuated by preventing S phase entry. LNCaP cells arrested in G_0/G_1 by serum starvation also exhibited reduced sensitivity to **2** as compared to cells grown in normal media. The finding that cytoxicity is partially rescued by MG132 treatment and G_0/G_1 arrest suggests RPB1 degradation contributes to cytotoxicity, however, contributions from other DNA dependent processes are not ruled out.

While transcription inhibition can activate p53 signaling, both events can be caused by DNA damage. Analysis of previously published microarray data revealed the induction of several p53 target genes in LNCaP cells cotreated with DHT and **1** (12). Further validation of transcript levels of these genes in this study also showed a time dependent increase in the expression of *GADD45A, MDM2, IGFBP3, P21, BAX* and *DDIT3* (Fig. 3.4A). Since these genes are also markers of genotoxic stress (38), and were found to be induced in A549 cells treated with alkylating polyamide derivatives (39), we searched for signs of DNA damage to determine if it was causing transcription inhibition and p53 activation. Interestingly, both comet assay and immunblot analysis of cellular DNA damage markers showed no significant signs of DNA damage. While faint phosphorylation of γH2A.X was visible, it is likely caused by cellular apoptosis as indicated by the concurrent PARP cleavage. This data is consistent with studies in yeast mutants that are hypersensitive to DNA damage which showed no increased sensitivity to polyamide treatment, suggesting these reversible DNA binders do not compromise genomic integrity (42).

The activation of p53 by transcription inhibition in the absence of DNA damage has been observed for DNA independent inhibitors of RNAP2 such as DRB, alpha-amanitin, and various RNAP2 targeted antibodies (5, 6, 40). Distamycin A, the natural

product which provided the structural inspiration for Py-Im polyamides, inhibits the initiation of RNA synthesis in cell-free assays (43). In cell culture, distamycin also induces degradation of RPB1 and activates p53 (44, 45). However, low antitumor potency and poor stability limit its utility.

To assess the therapeutic potential of polyamide **1** as an antitumor agent, LNCaP xenografts in a murine model were treated with **1** or PBS vehicle. After three rounds of treatment, tumor growth was found to be reduced by 64% in the treated group. While treatment with **1** alone did not cause changes in animal body weight or obvious signs of toxicity in tumor free animals, treatment in tumor bearing animals resulted in weight loss after three treatments. The accompanied elevation in serum uric acid may be an indication of tumor lysis syndrome (46) that is associated with rapid tumor cell turnover upon polyamide treatment. We anticipate that Py-Im polyamides could also demonstrate efficacy in additional xenograft models.

References

1. Derheimer FA, Chang CW, & Ljungman M (2005) Transcription inhibition: A potential strategy for cancer therapeutics. *European Journal of Cancer* 41(16):2569-2576.
2. Koumenis C & Giaccia A (1997) Transformed cells require continuous activity of RNA polymerase II to resist oncogene-induced apoptosis. *Molecular and cellular biology* 17(12):7306-7316.
3. Jung Y & Lippard SJ (2006) RNA polymerase II blockage by cisplatin-damaged DNA - Stability and polyubiquitylation of stalled polymerase. *Journal of Biological Chemistry* 281(3):1361-1370.
4. Ljungman M & Zhang FF (1996) Blockage of RNA polymerase as a possible trigger for uv light-induced apoptosis. *Oncogene* 13(4):823-831.
5. Ljungman M, Zhang FF, Chen F, Rainbow AJ, & McKay BC (1999) Inhibition of RNA polymerase II as a trigger for the p53 response. *Oncogene* 18(3):583-592.
6. Arima Y, *et al.* (2005) Transcriptional blockade induces p53-dependent apoptosis associated with translocation of p53 to mitochondria. *Journal of Biological Chemistry* 280(19):19166-19176.
7. Nguyen VT, *et al.* (1996) In vivo degradation of RNA polymerase II largest subunit triggered by alpha-amanitin. *Nucleic acids research* 24(15):2924-2929.
8. Arseneau JC, *et al.* (1972) Nonlymphomatous malignant tumors complicating Hodgkin's disease. Possible association with intensive therapy. *The New England journal of medicine* 287(22):1119-1122.
9. Dervan PB & Edelson BS (2003) Recognition of the DNA minor groove by pyrrole-imidazole polyamides. *Current opinion in structural biology* 13(3):284-299.
10. Chenoweth DM & Dervan PB (2009) Allosteric modulation of DNA by small molecules. *Proceedings of the National Academy of Sciences of the United States of America* 106(32):13175-13179.
11. Chenoweth DM & Dervan PB (2010) Structural Basis for Cyclic Py-Im Polyamide Allosteric Inhibition of Nuclear Receptor Binding. *Journal of the American Chemical Society* 132(41):14521-14529.
12. Nickols NG & Dervan PB (2007) Suppression of androgen receptor-mediated gene expression by a sequence-specific DNA-binding polyamide. *Proceedings of the National Academy of Sciences of the United States of America* 104(25):10418-10423.
13. Nickols NG, Jacobs CS, Farkas ME, & Dervan PB (2007) Modulating hypoxia-inducible transcription by disrupting the HIF-1-DNA interface. *ACS chemical biology* 2(8):561-571.
14. Muzikar KA, Nickols NG, & Dervan PB (2009) Repression of DNA-binding dependent glucocorticoid receptor-mediated gene expression. *Proceedings of the National Academy of Sciences of the United States of America* 106(39):16598-16603.

15. Matsuda H*, et al.* (2011) Transcriptional inhibition of progressive renal disease by gene silencing pyrrole-imidazole polyamide targeting of the transforming growth factor-beta 1 promoter. *Kidney International* 79(1):46-56.
16. Synold TW*, et al.* (2012) Single-dose pharmacokinetic and toxicity analysis of pyrrole-imidazole polyamides in mice. *Cancer Chemother Pharmacol*.
17. Raskatov JA*, et al.* (2012) Gene expression changes in a tumor xenograft by a pyrrole-imidazole polyamide. *Proceedings of the National Academy of Sciences of the United States of America* 109(40):16041-16045.
18. Best TP, Edelson BS, Nickols NG, & Dervan PB (2003) Nuclear localization of pyrrole-imidazole polyamide-fluorescein conjugates in cell culture. *Proceedings of the National Academy of Sciences of the United States of America* 100(21):12063-12068.
19. Meier JL, Montgomery DC, & Dervan PB (2012) Enhancing the cellular uptake of Py-Im polyamides through next-generation aryl turns. *Nucleic acids research* 40(5):2345-2356.
20. Puckett JW, Green JT, & Dervan PB (2012) Microwave Assisted Synthesis of Py-Im Polyamides. *Organic letters* 14(11):2774-2777.
21. Raskatov JA, Hargrove AE, So AY, & Dervan PB (2012) Pharmacokinetics of Py-Im Polyamides Depend on Architecture: Cyclic versus Linear. *Journal of the American Chemical Society* 134(18):7995-7999.
22. Dai KS*, et al.* (2005) An evaluation of clinical accuracy of the EasyTouch blood uric acid self-monitoring system. *Clinical Biochemistry* 38(3):278-281.
23. Nowak DE, Tian B, & Brasier AR (2005) Two-step cross-linking method for identification of NF-kappaB gene network by chromatin immunoprecipitation. *Biotechniques* 39(5):715-725.
24. Reddy TE*, et al.* (2009) Genomic determination of the glucocorticoid response reveals unexpected mechanisms of gene regulation. *Genome Res* 19(12):2163-2171.
25. Langmead B, Trapnell C, Pop M, & Salzberg SL (2009) Ultrafast and memory-efficient alignment of short DNA sequences to the human genome. *Genome Biology* 10(3).
26. Yu JD*, et al.* (2010) An Integrated Network of Androgen Receptor, Polycomb, and TMPRSS2-ERG Gene Fusions in Prostate Cancer Progression. *Cancer cell* 17(5):443-454.
27. Zhang Y*, et al.* (2008) Model-based Analysis of ChIP-Seq (MACS). *Genome biology* 9(9):R137.131.
28. de Hoon MJ, Imoto S, Nolan J, & Miyano S (2004) Open source clustering software. *Bioinformatics* 20(9):1453-1454.
29. Saldanha AJ (2004) Java Treeview--extensible visualization of microarray data. *Bioinformatics* 20(17):3246-3248.
30. Diamond RA & DeMaggio S (2000) *In living color : protocols in flow cytometry and cell sorting* (Springer, Berlin ; New York) pp xxv, 800 p.
31. Zisman A*, et al.* (2003) LABAZ1: A metastatic tumor model for renal cell carcinoma expressing the carbonic anhydrase type 9 tumor antigen. *Cancer research* 63(16):4952-4959.

32. Dose C, Farkas ME, Chenoweth DM, & Dervan PB (2008) Next generation hairpin polyamides with (R)-3,4-diaminobutyric acid turn unit. *Journal of the American Chemical Society* 130(21):6859-6866.
33. Palstra RJ, *et al.* (2008) Maintenance of Long-Range DNA Interactions after Inhibition of Ongoing RNA Polymerase II Transcription. *PloS one* 3(2).
34. Bregman DB, *et al.* (1996) UV-induced ubiquitination of RNA polymerase II: a novel modification deficient in Cockayne syndrome cells. *Proceedings of the National Academy of Sciences of the United States of America* 93(21):11586-11590.
35. Ratner JN, Balasubramanian B, Corden J, Warren SL, & Bregman DB (1998) Ultraviolet radiation-induced ubiquitination and proteasomal degradation of the large subunit of RNA polymerase II - Implications for transcription-coupled DNA repair. *Journal of Biological Chemistry* 273(9):5184-5189.
36. Aune GJ, *et al.* (2008) Von Hippel-Lindau - Coupled and Transcription-Coupled Nucleotide Excision Repair - Dependent Degradation of RNA Polymerase 11 in Response to Trabectendin. *Clinical Cancer Research* 14(20):6449-6455.
37. McKay BC, Becerril C, Spronck JC, & Ljungman M (2002) Ultraviolet light-induced apoptosis is associated with S-phase in primary human fibroblasts. *DNA Repair* 1(10):811-820.
38. El-Deiry WS (1998) Regulation of p53 downstream genes. *Seminars in Cancer Biology* 8(5):345-357.
39. Kashiwazaki G, *et al.* (2012) Synthesis and biological properties of highly sequence-specific-alkylating N-methylpyrrole-N-methylimidazole polyamide conjugates. *Journal of medicinal chemistry* 55(5):2057-2066.
40. Derheimer FA, *et al.* (2007) RPA and ATR link transcriptional stress to p53. *Proceedings of the National Academy of Sciences of the United States of America* 104(31):12778-12783.
41. Carlson CD, *et al.* (2010) Specificity landscapes of DNA binding molecules elucidate biological function. *Proceedings of the National Academy of Sciences of the United States of America* 107(10):4544-4549.
42. Marini NJ, *et al.* (2003) DNA binding hairpin polyamides with antifungal activity. *Chemistry & biology* 10(7):635-644.
43. Puschendorf B, Petersen E, Wolf H, Werchau H, & Grunicke H (1971) Studies on the effect of distamycin A on the DNA dependent RNA polymerase system. *Biochem Biophys Res Commun* 43(3):617-624.
44. Zhang Z, *et al.* (2009) Tanshinone IIA triggers p53 responses and apoptosis by RNA polymerase II upon DNA minor groove binding. *Biochem Pharmacol* 78(10):1316-1322.
45. Hirota M, Fujiwara T, Mineshita S, Sugiyama H, & Teraoka H (2007) Distamycin A enhances the cytotoxicity of duocarmycin A and suppresses duocarmycin A-induced apoptosis in human lung carcinoma cells. *Int J Biochem Cell Biol* 39(5):988-996.
46. Coiffier B, Altman A, Pui CH, Younes A, & Cairo MS (2008) Guidelines for the management of pediatric and adult tumor lysis syndrome: An evidence-based review. *Journal of Clinical Oncology* 26(16):2767-2778.

3.5 Supplemental Material

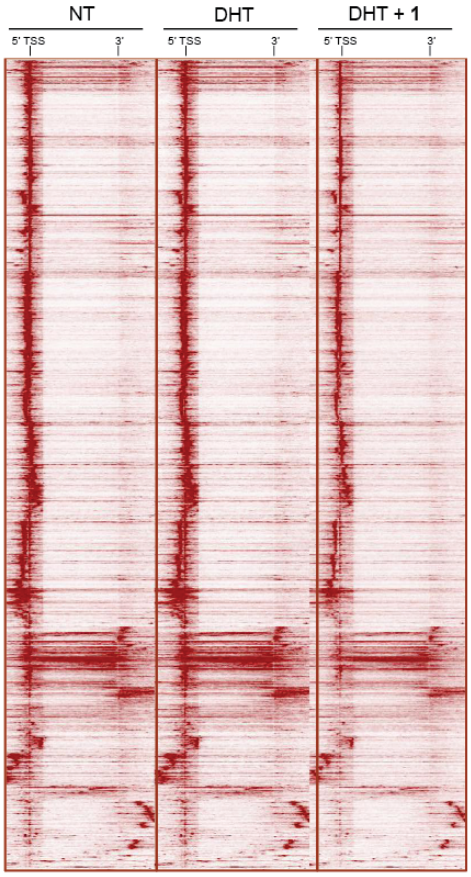

Figure S3.1. Heat map of global distribution of RNAP2 over gene bodies.

A

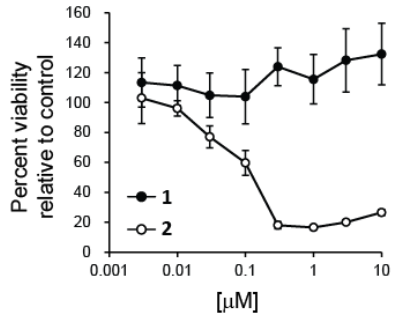

B

Polyamides	5'- CGA **TGTTCA** AGC -3' T_m / °C	ΔT_m / °C
—	53.1 (±0.2)	—
1	68.3 (±0.2)	15.2
2	71.0 (±0.4)	17.9

C

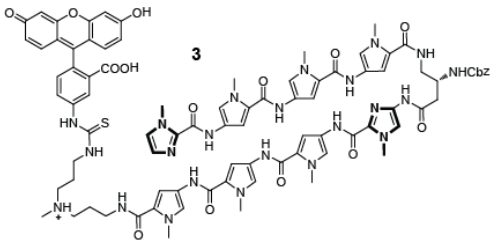

D

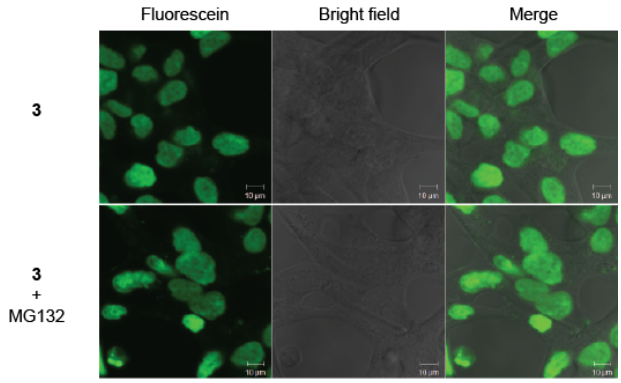

E

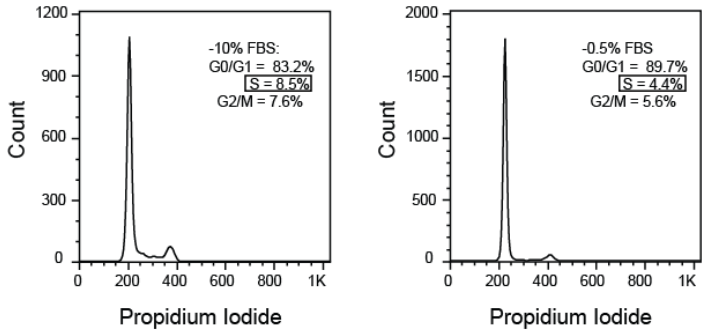

Figure S3.2 (**A**) Cytotoxicity of **1** and **2** in LNCaP cells after 24h treatment. Although **1** demonstrates cytotoxicity at 72h, minimal cytotoxicity is seen at 24h. (**B**) DNA thermal stability analysis of **1** and **2** show comparable DNA binding of the two compounds. (**C**) Chemical structure of fluorescein conjugated form (**3**) of polyamide **2.** (**D**) Addition of MG132 did not affect the cellular uptake of **3**. (**E**) Serum starvation decreases the percent of LNCaP Cells in S phase.

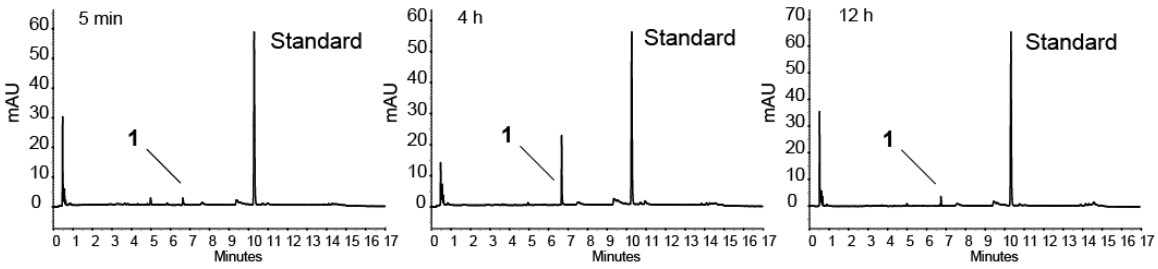

Figure S3.3 Circulation study of **1**in C57BL/6J mice (n=4) at 5min, 4h, and 12h post subcutaneous injection in 5% DMSO in PBS.

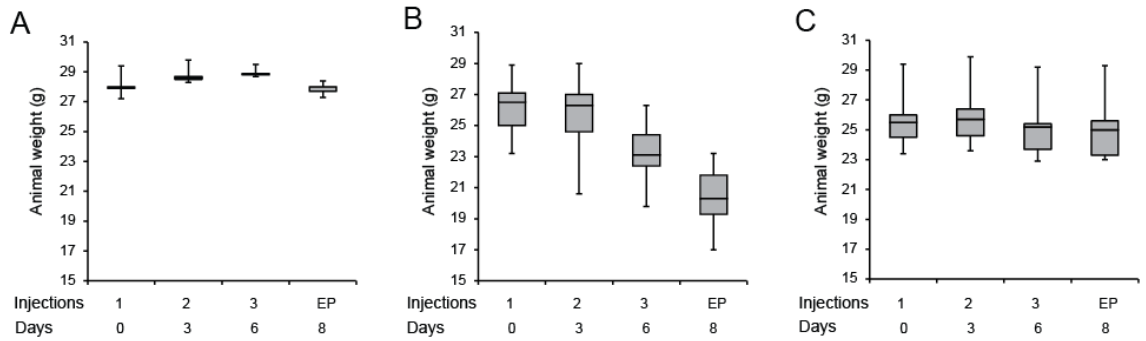

Figure S3.4 Animal weights were measured at each injection of **1** and at the experiment endpoint (EP). (**A**) Weight measurements of tumor free male immunocompromized mice treated with 20nmol of **1** once every 3 days for 3 injections (n=5). (**B**) Weight measurements of LNCaP tumor bearing male immunocompromized mice treated with 20nmol of **1** once every 3 days for 3 injections (n=12). (**C**) Weight measurements of LNCaP tumor bearing male immunocompromized mice treated with vehicle (5% DMSO in PBS) once every 3 days for 3 injections (n=13). Experiments were end pointed 2 days after the last injection. Error bars represents max and min, boxes represents the upper and lower quartiles and median.

Gene	**Forward (5'-3')**	**Reverse (5'-3')**
P21	GCCATTAGCGCATCACAGT	ACCGAGGCACTCAGAGGAG
GADD45a	GCAGGATCCTTCCATTGAGA	CTCTTGGAGACCGACGCTG
MDM2	CTGATCCAACCAATCACCTG	AAGCCTGGCTCTGTGTGTAA
IGFBP3	CGGTCTTCCTCCGACTCAC	CTCTGCGTCAACGCTAGTGC
BAX	CAGCCCATGATGGTTCTGAT	GACATGTTTTCTGACGGCAA
RPB1	CTCAATCACCCCCTGCC	GAGTCCTGAGTCCGGATGAA
GUSB	CTCATTTGGAATTTTGCCGATT	CCGAGTGAAGATCCCCTTTTT

Table S3.1 Primer sequences used for qPCR experiments

Chapter 4

Animal toxicity of hairpin pyrrole-imidazole polyamides varies with the turn unit

The text of this chapter is taken from a manuscript coauthored with Nicholas G. Nickols[a,b], Benjamin C. Li[a], Jerzy O. Szablowski[a], Shari R. Hamilton[c], Jordan L. Meier[a], Chieh-Mei Wang[a], and Peter B. Dervan[a]

[a] *Division of Chemistry and Chemical Engineering, California Institute of Technology, Pasadena, CA*
[b] *Department of Radiation Oncology, David Geffen School of Medicine at UCLA, Los Angeles, CA*
[c] *IDEXX RADIL, Columbia, MO 65021, USA*

(Yang, F., Nickols, N.G., Li, B.C., Szablowski, J. O., Hamilton, S. R., Meier, J. L., Wang, C., and Dervan, P.B. (2013) *Manuscript in preparation*)

Abstract

A hairpin pyrrole-imidazole polyamide targeted to the androgen receptor consensus half-site (DNA sequence 5'-WGWWCW-3', W=A or T) was found to exert antitumor effects against prostate cancer cells in culture and in xenografts. Previously, a single administration of the compound, hairpin **1,** which has a chiral amine at the α position of the γ-aminobutyric acid turn (γ-turn) unit, was found to have no adverse effects toward wild type mice at 2.5 and 5 mg/kg, however, dose escalation to 10 mg/kg caused significant weight loss. In the same study, hairpin **4**, which has an acetamide at the β position of the γ-turn unit resulted in increased animal morbidity at 2.3 and 5.4 mg/kg. To identify structural motifs that cause animal toxicity in our lead molecule we synthesized four polyamides **1-4** with varying amino or acetamide substitution at the α and β positions in the γ-turn unit. Weight loss, organ histopathology, and serum chemistry were analyzed in wild type mice after compound administration. While serum bioavailability was similar for all four polyamides after subcutaneous injection, toxicity varied greatly between the four polyamides. Dose limiting liver toxicity was observed for polyamides **1**, **2**, and **4**, but not polyamide **3**, with an acetamide at the α position. Hairpin **3** demonstrates no significant evidence of rodent toxicity with a single subcutaneous injection up to 10 mg/kg, or after repeated dosing at 1 mg/kg by histopathology and serum analysis. This compound is cytotoxic to LNCaP cells in cell culture and increases p53 activity without inducing detectable DNA damage by comet assay, and demonstrates antitumor activity against prostate tumor xenografts at a dose level with no detectable pathology.

4.1 Introduction

Prostate cancer is a major contributor of cancer death in American males.(1) The malignant transformation of prostate epithelial tissue is caused by an altered pattern of gene expression driven by the androgen receptor (AR). Clinically, localized prostate cancer is curable by surgery or radiation.(2, 3) Advanced prostate cancer is treated with systemic therapies that target testosterone signaling (enzalutamide, abiraterone), immunotherapy (sipuleucel T), and taxane-based chemotherapy (docetaxel, cabazitaxel).(4) These new agents have shown survival benefits to patients with castration resistant, metastatic disease. However, all patients will eventually progress on these drugs. Resistance to the second-generation antiandrogen enzalutamide and the CYP17 inhibitor abiraterone may be due to the action of splice variants of AR that lack the ligand-binding domain (AR-V).(5, 6) Therefore, therapy resistant prostate cancer is an unmet clinical need, and novel systemic therapies are needed in patients after these treatments have failed.(4)

Direct interference of AR driven transcription at the protein-DNA interface is a strategy that can circumvent resistance conferred by AR-V. Genomic DNA is the predominant target of many chemo- and radio- therapies. The interactions of these therapies with DNA result in the inhibition of DNA-dependent processes that are over-active in cancer cells such as transcription.(7-9) While AR driven transcription can be inhibited by DNA targeted agents,(10, 11) most conventional DNA-targeted therapeutics are genotoxic and can induce secondary malignancies.(12) DNA-damaging agents may also contribute to tumor metastasis through effects on non-cancerous cells in the tumor

microenvironment.(13) Small molecules that interact with DNA without genotoxicity could be a significant advance over conventional DNA-targeted therapeutics.

Pyrrole (Py) – Imidazole (Im) polyamides are minor groove binders that have been shown to affect gene expression in a number of inducible transcription systems. (14-20) As non-covalent DNA-binding oligomers, these compounds form specific hydrogen bonds to the minor groove floor with programmable sequence recognition and high affinity. (21-23)

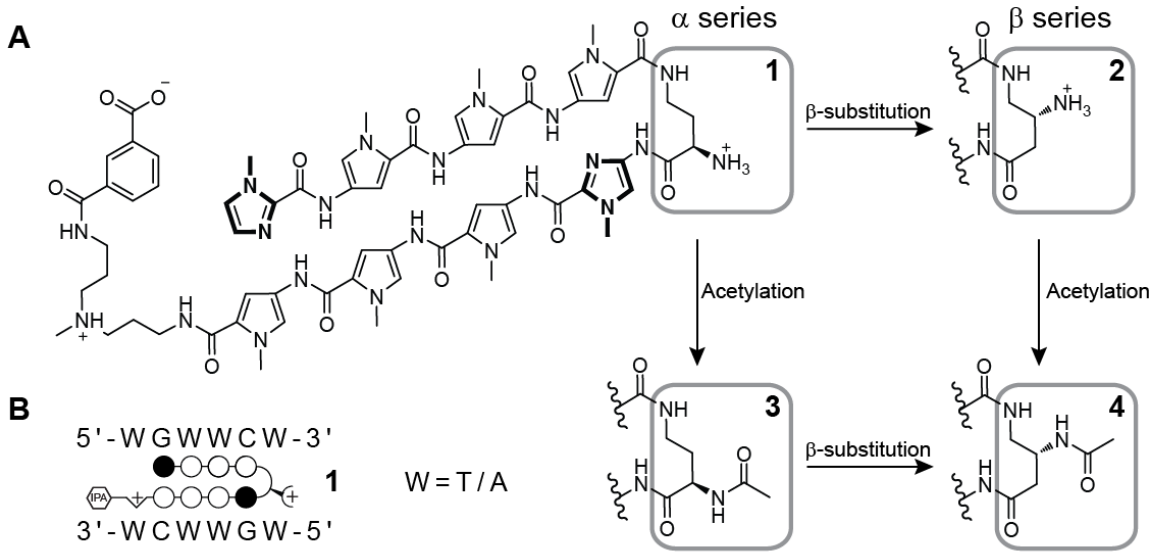

Figure 4.1. Chemical structures. **(A)** Structures of polyamides **1**-**4**. The compounds only vary by the amino substitution on the g-turn unit. **(B)** The prefered DNA binding sequence of the polyamide core. Polyamide **1** is shown bound to the sequence 5'-WGWWCW-3'. Closed circles represent imidazole units and open circles represent pyrrole units.

Py-Im polyamides are toxic to a variety of cancer cell lines, including prostate cancer, and exhibit no apparent genotoxicity.(24) A typical hairpin oligomer consists of eight aromatic amino acid rings joined in the middle by a γ-aminobutyric acid (γ-turn). (25) While sequence recognition is predominately directed by the antiparallel pairing of N-methylpyrrole and N-methylimidazole carboxamides, structural modifications to the γ-turn, such as substitution at the prochiral α and β positions, have been shown to influence

the DNA affinity,(26) cell uptake, and the biological activity of polyamides in both cell culture and animals.(27, 28)

To date, we have reported the pharmacokinetic (PK) profiles of two eight-ring hairpin-polyamides targeted to the sequence 5'-WGWWCW-3' (W=A or T) in mice. The compounds **1** and **4** (Fig. 4.1) differ in structure at the γ-turn and were found to have distinct PK profiles. Both compounds were bioavailable in serum after intravenous injection for more than 24 hours, however **4** was found to have longer retention in both the serum and tissues. Both compounds were minimally excreted through the feces, but significant renal clearance was exclusive to **4.**(28) In addition to differences in the PK profiles, **1** and **4** also exhibited different degrees of toxicity to female C57BL/6J mice. While single subcutaneous administrations of **1** in female mice at 2.5 mg/kg and 5 mg/kg did not adversely affect the animals, escalated dosing to 10 mg/kg resulted in weight loss greater than 15%. In comparison, **4** caused acute animal toxicity in addition to weight loss at 2.3 mg/kg and 4.5 mg/kg.(28) To dissect the differences in toxicities, there are two variables on the turn that must be sorted out (α versus β position and amino versus acetamide substitution).

More recently compound **1** was found to suppress the growth of LNCaP xenografts in immunocompromised mice after three subcutaneous injections at 1 mg/kg.(24) Thus, a systematic toxicity study of **1** and related polyamides with modifications to the γ-turn may yield structures with reduced animal toxicity. In addition, an extensive toxicity study of polyamides in animals to identify target organs of pathology is a necessary step towards translation of this technology into the clinic.

In this paper, we report the animal toxicity of four structurally related polyamides with identical Py-Im sequence but with different substitutions at the γ-turn (Fig. 4.1), a change that does not alter binding sequence preference. We assessed mouse weight, organ histopathology, and serum chemistry in wild type male mice after single and multiple dosing regimens. Dose limiting toxicity was observed at the highest dose for three of the four molecules. From this study, we have identified one polyamide that demonstrates no detectable toxicity by histopathology or serum analysis after single or repeated subcutaneous injections.

4.2 Materials and Methods

Synthesis of polyamides. Py-Im polyamides **1-4** and **6-9** were synthesized on Kaiser oxime resin (Novabiochem) as previously described.(15, 29) Complete oligomers were cleaved from resin using 3,3'-diamino-N-methyl-dipropylamine and purified by reverse-phase HPLC in 0.1% aqueous TFA and acetonitrile.(30) Isophthalic acid and fluorescein isothiocyanate conjugates were synthesized as previously described.(31) Cyclic polyamide **5** was synthesized on 2-Chlorotrityl chloride resin (Bachem) as previously described.(32) Deprotection of the γ-turn was performed as described.(26) Hairpin polyamides **3, 4, 8,** and **9** were acetylated as previously described.(26, 33) Polyamides **1-9** were purified again by reverse phase HPLC after final conjugation. All polyamide purity and molecular weight were measured by analytical HPLC and MALDI-ToF mass spectrometry, respectively (Table S4.1).

Chemicals and animals. Ten percent neutral buffered formalin was purchased from Richard-Allan Scientific. Six to eight week old male C57BL/6J mice were purchased from Jackson labs.

Thermal denaturation assay. Thermal stabilization of the DNA oligo 5'-TTGCTGTTCTGCAA-3' by **1-4** (target sequence underlined) was determined as previously described. (26)

Animal weight loss analysis. All animal experiments were conducted under an approved protocol at the California Institute of Technology. Animals were allowed to adjust for 3 days after arrival before treatment. Compounds were quantified with a UV/Vis spectrophotometer using extinction coefficient of 69500 $M^{-x} \cdot cm^{-c}$ at λ_{max} near 315 nm. For single injection weight loss experiments, the animals were separated into 3 treatment groups receiving 1 mg/kg, 3 mg/kg, or 10 mg/kg of compound in up to 200 μL of a 25% DMSO/saline vehicle, with 4 animals per group. Animals were monitored daily for weight loss over 9 days and sacrificed. For repeated injection experiments the animals were separated into groups of 3 and injected with 1 mg/kg of 1-4 once every 3 days and sacrificed two days after the last injection. Weight was recorded on days of injection and at the experiment endpoint.

Animal histopathology analysis. Sacrificed animals from weight loss experiments were fixed in 10% formalin and sent for histopathology analysis by IDEXX-RADIL. Histopathologic analysis was performed on the cecum, duodenum, heart, ileum, kidney, liver, lung, pancreas, spleen, and stomach. Tissue analysis was performed as a blind study to the identity of the animals.

Serum analysis. Serum from treated animals were collected by retroorbital bleeding. Blood samples were centrifuged at 6,000 rpm for 5 min to collect the serum. Serum ALT, AST, total bilirubin, BUN, and creatinine levels were sent for analysis by IDEXX-RADIL. Serum analysis was performed as a blind study to the identity of the animals.

For hematology analysis, blood was collected from 5 male C57BL6/J mice by retroorbital bleed and sent for hematological analysis in K_2EDTA coated BD Microcontainers™. The animals were allowed to recover for 1 week before treatment with **2** using the same injection conditions as the NSG mice. At the treatment endpoint the animals were bled again and euthanized. Blood samples for serum chemistry analysis and hematology analysis were prepared separately. All samples were sent for analysis at IDEXX-RADIL.

Liver microsomal stability analysis. Liver microsomal stability of 1-4 was performed by Apredica. Briefly, each polyamide was incubated with 1 mg/ml human or mouse microsomes at 37 ^{o}C. The reaction was incubated in 100 mM KH_2PO_4, 2mM NADPH, 3mM $MgCl_2$ at pH 7.4. Samples were also incubated in the absence of NADPH to detect NADPH-free degradation. After 60 min the samples were mixed with an equal volume of ice cold methanol stop solution. The mixture was allowed to sit on ice for at least 10 min and mixed with an equal volume of water. The samples were then centrifuged to remove the precipitates and the samples were analyzed by LC/MS/MS. Data represents % remaining by comparing with time zero concentration. The experiments were performed in duplicate.

Tissue distribution of fluorescein tagged polyamides. Male C57BL/6J mice (n=2 per group) were injected with 50 nmol (~3 mg/kg) of **6-9** and then sacrificed 24 hours later. Tissue was excised and processed as previously described. (20) Fluorescence intensity in liver tissue was assessed by laser confocal microscopy in 10 μm thick sections.

Cell Viability Assays. LNCaP cells were plated in clear bottom 96-well plates at 5,000–7,500 cells per well and allowed to adhere for 36–48 h. Compounds were then added in fresh media. Cell metabolic activity was determined by the WST-1 assay (Roche) after

72-h incubation with cells. Quantification was performed on a Perkin Elmer Victor 3 plate reader. Assays were performed in biological triplicates.

Protein ELISA Assays. Cellular levels of RPB1 and p53 protein in LNCaP cells after treatment with 10 μM **2** for 72 h were determined by ELISA. Cells treated with DMSO vehicle and 1 μM doxorubicin for 24 h were used as control. Cellular RBP1 levels were determined by a RPB1 specific ELISA kit (Cusabio Life Sciences) according to manufacturer's instructions. Total cellular p53 protein level was determined with a pan-p53 ELISA kit (Roche) according to manufacturer's instructions. Assays were performed in biological triplicates.

Quantitative RT-PCR. LNCaP cells were plated in 12 well plates at 50,000 cells per well and allowed to adhere for 36-48 h. The cells were then treated with 1, 3, and 10 μM of **2** for 72 h. Total cellular RNA was extracted using RNEasy columns (Qiagen) following the manufacturer's protocols. Isolated RNA was reverse transcribed with Transcriptor First Strand cDNA kit (Roche). Quantitative real-time PCR was performed using SYBR Green PCR Master Mix (Applied Biosystems) on an ABI 7300 instrument. Amplification of *p21, IGFBP3,* and *GADD45A* cDNA was measured relative to β-glucuronidase using previously published primers. Experiments were performed in biological replicates.

Comet Assay. LNCaP cells were plated in 6 well plates at 100,000 cells per well and allowed to adhere for 36–48 h. The cells were then incubated with either 10 μM **2** for 48 h or 5 μM doxorubicin for 4 h. DNA damage was assayed using the Trevigen CometAssay system. Cells were harvested by gentle aspiration with PBS and prepared on slides according to the manufacturer's protocol. Comets slides were imaged on a

confocal microscope (Exciter, Zeiss) at 10× magnification. Images were scored using Comet Assay Lite IV (Perceptive Instruments). More than 100 comets were scored for each condition. DNA damage is reported as percentage of DNA in the tail.

In Vivo Xenograft Experiments. Mice experiments were conducted under an approved protocol by the Institutional Animal Care and Use Committee of the California Institute of Technology. Male C57BL6/J mice and male NSG mice were purchased from The Jackson Laboratory. All animals were maintained on a standard light-dark cycle. LNCaP cells (2.5 million cells) were engrafted in a mixture of 1:1 media and matrigel in the left flank of NSG mice. Tumors were allowed grow to ~200 mm^3 ($0.5 \times L \times W^2$) before treatment. Py-Im polyamide **2** was administered by SC injection once every 3 d at 1 mg/kg in a 20% (vol/vol) DMSO:Normal saline vehicle solution for 6 injections. Animals were sacrificed two days after the final injection. Animal weight and general health were monitored daily. Fourteen animals were used for each treatment group.

4.3 Results

Selection of polyamides. We synthesized four structurally related polyamides (Fig. 4.1) that have an identical Py-Im sequence. These polyamides demonstrate thermal stabilization of DNA duplexes containing their target sequence (Fig. S4.1). Polyamide **1**, ImPyPyPy-2-$(R)^{H2N}\gamma$-ImPyPyPy~NHMe~IPA, suppressed LNCaP xenografts in mice.(24) Polyamide **2**, ImPyPyPy-3-$(R)^{H2N}\gamma$-ImPyPyPy~NHMe~IPA, differs from **1** in that the γ-turn is substituted at the β position. Polyamide **3**, ImPyPyPy-2-$(R)^{AcHN}\gamma$-ImPyPyPy~NHMe~IPA, differs from **1** in that the primary amine is acetylated. Polyamide **4**, ImPyPyPy-3-$(R)^{AcHN}\gamma$-ImPyPyPy~NHMe~IPA, incorporates both changes from **2** and **3**. Our previous report in female mice showed **1** and **4** both circulated in

serum after intravenous injection.(28) To determine if **1-4** demonstrated comparable serum levels after subcutaneous injection, male C57BL/6J mice were injected with 10 mg/kg each of **1-4** and blood collected by retroorbital bleed at various time points. All polyamides were bioavailable and detectable up to 24 h after subcutaneous injection (Fig. S4.2).

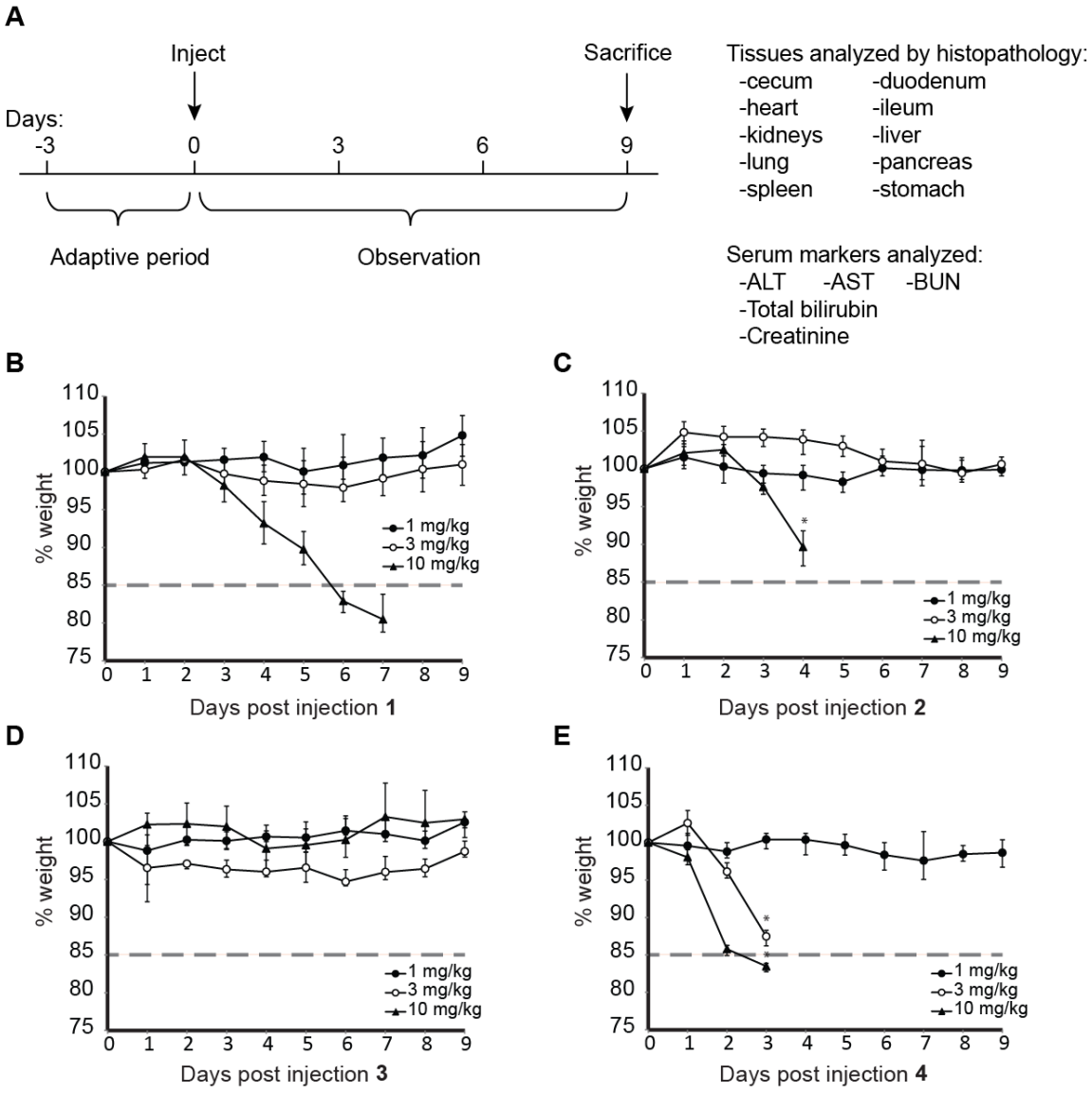

Figure 4.2. Experiment set up of single dose weight curve experiments. **(A)** Male C57BL/6J mice were allowed to adapt to new cage settings for 3 days after arrival and then treated with compound. Animal weights were then monitored for 9 days. Humane endpoint was defined by visible signs of duress in the animals or weight loss in excess of 15% of original body weight. Weight curves of compounds **(B) 1, (C) 2, (D) 3, and (E) 4.**

Escalating Single Dose Subcutaneous Injections. To determine the acute effects of subcutaneous dosing of **1-4** and dose-limiting organ toxicities, 8 week-old male C57BL/6J mice (n=4 per dosing group) were treated with 1, 3, 10 mg/kg **1-4** and observed for 9 days and then sacrificed (Fig. 4.2). Representative mice (n=2 per dosing group unless otherwise noted) were subjected to histopathology analysis by a veterinary pathologist. Blood from all mice was sampled and sent for analysis of serum markers of target organs. Mice treated with **1** and **2** demonstrated significant weight loss only at 10 mg/kg. Polyamide **4** was only tolerated at 1 mg/kg; all mice treated with **4** at 3 or 10 mg/kg exhibited hunched posture, loss of mobility, and acute morbidity. Mice treated with polyamide **2** at 10 mg/kg demonstrated similar morbidity. These mice were euthanized when significant duress was apparent. All other mice, including those treated with **1** at 10 mg/kg and **3** at all concentrations, demonstrated no change in behavior and appearance.

Histopathology revealed lesions consistent with toxicity in the liver, kidney and spleen in animals receiving a single injection of polyamides **1**, **2** and **4**. The most severe lesions characterized by diffuse hepatocellular necrosis and apoptosis or multifocal bridging hepatocellular necrosis and apoptosis were identified in animals treated with polyamide **2** at 10 mg/kg and polyamide **4** at both 3 and 10 mg/kg, respectively. Mild hepatocellular necrosis and apoptosis was observed in animals treated with polyamide **1** at doses of 3 and 10 mg/kg, polyamide **2** at 3 mg/kg and polyamide **4** at 1 mg/kg (Fig. 4.3A). Moderate atypical tubular regeneration (karyomegaly, tubular attenuation, mitotic figures) and/or tubular epithelial necrosis and apoptosis were seen in the kidneys in animals treated with polyamide **2** at 3 mg/kg and polyamide **4** at 3 and 10 mg/kg (Fig.

4.3B). Milder tubular regeneration and karyomegaly was observed in animals treated with polyamide **1** at 10 mg/kg and polyamide **4** at 1 mg/kg. Mild lymphoid apoptosis in the white pulp of the spleen was noted in animals treated with polyamide **2** at 10 mg/kg and polyamide **4** at 3 and 10 mg/kg. Polyamide **3** demonstrated no detectable toxicity at any dose level tested. No lesions consistent with toxicity were observed in the gastrointestinal tract, heart, lung, pancreas, or stomach in any animals.

Because toxicity to the liver and kidneys were identified as the target organs at risk, serum markers for these organ systems were measured (Fig. 4.3C). Mice treated with polyamide **1** demonstrated significant elevation of AST, ALT, and total bilirubin at 10 mg/kg, indicative of acute damage to liver cells, and moderate elevation of ALT at 3 mg/kg. Elevation of creatinine and blood urea nitrogen (BUN) was not observed for any dose level of **1**. Polyamide **2** treated mice had severe elevation of AST, ALT, and total bilirubin at 10 mg/kg and to a lesser extent at 3 mg/kg. These mice also had elevated BUN at 10 mg/kg. Mice treated with polyamide **4** demonstrated marked and severe elevations of AST, ALT, and total bilirubin at both 3 mg/kg and 10 mg/kg. In addition, these mice had significantly elevated creatinine and BUN at 10 mg/kg, and elevated BUN at 3 mg/kg. Mice treated with polyamide **3** demonstrated no elevation of these markers at the dose levels tested.

A

Necropsy analysis of mice cadavers after single SC injection of polyamide.

		Organ									
Compound	Dose (mg/kg)	Cecum	Duodenum	Heart	Ileum	Kidney	Liver	Lung	Pancreas	Spleen	Stomach
1	1*										
	3						+				
	10					+	+				
2	1*										
	3					++	+				
	10						+++			+	
3	1*										
	3										
	10										
4	1*					+	+				
	3					++	+++			+	
	10*					++	+++			+	

B

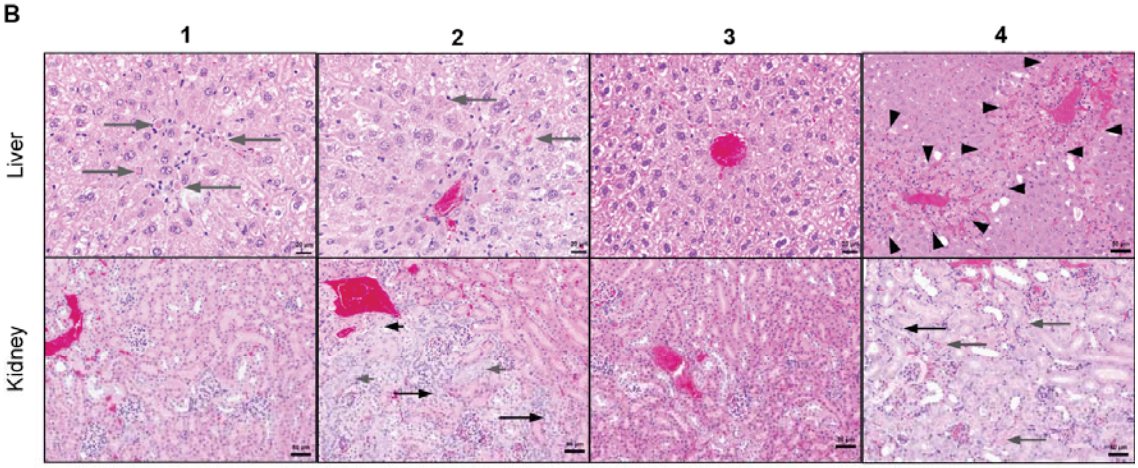

C

Serum chemistry analysis

Compound	mg/kg	ALT (U/L)	AST (U/L)	T Bili. (mg/dL)	BUN (mg/dL)	Creat. (mg/dL)
1	1	112±14	68±13	0.1	32±2	0.2
	3	421±47	177±16	0.2	38±1	0.2
	10	1867±515	2282±561	8.7±0.4	27±1	0.4
2	1	106±68	85±11	0.2	29±1.5	0.2
	3	1096±638	492±192	0.23	28.5±2.6	0.28
	10	18312±2414	15405±1441	4.3±0.5	91.3±29.6	0.3±0.1
3	1	36±4.2	93±41	0.2	27±1	0.2
	3*	29±2.8	47±2.1	0.2	35±4	0.3
	10	26±2.6	47±3.7	0.1	29±2	0.2
4	1	162±188	160±180	0.1	28±2.5	0.2
	3*	10404±235	5976±165	0.85	133±4.2	0.85±0.07
	10*	Insuff. Sample	10937±1408	2.5±0.2	138±8.5	1.3

Figure 4.3. **(A)** Histopathology analysis of sacrificed animals showed primary organ damage in the kidney and liver for compounds **1, 2,** and **4**. Animals treated with **3** did not exhibit signs of organ damage. * represents n=1. + = mild damage, ++ = moderate damage, +++ = severe damage. **(B)** Liver and kidney histopathology of two representative animals treated with compounds **1**-**4** at 3 mg/kg. **Liver:** long gray arrow=hepatocellular apoptosis/necrosis, arrowheads=outline area of bridging hepatocellular necrosis/apoptosis. **Kidney:** short gray arrow=tubular epithelial karyomegaly, long gray arrow=tubular epithelial apoptosis/necrosis, short black arrow=tubular epithelial mitoses, long black arrow=tubular epithelial attenuation. **(C)** Serum levels of liver damage and kidney damage markers. Significantly elevated markers are shaded in gray. * n=2.

In a previous circulation study, it was found that a cyclic form of a hairpin polyamide targeted to the sequence 5'-WGGWWW-3' had increased animal toxicity.(34) However, in addition to the motif change from hairpin to cycle, the γ-turn of the cyclic compound was also changed from a (R)-2,4-diaminobutyric acid turn to (R)-3,4-diaminobutyric acid turn. To determine if the toxicity is dependent on the polyamide shape or the γ-turn, we synthesized cyclic polyamide **5** (Fig. S4.3). The compound was found to be bioavailable after subcutaneous injection at 10 mg/kg and did not cause significant weight loss in animals. However compound **5** did affect the kidney and liver and caused levels of ALT and AST to increase in a dose dependent manner.

Multiple-Dose Subcutaneous Injections. In addition to single dose injections, the effects of repeated dosing of polyamides **1-4** in mice were examined. In this experiment, 8 week-old male C57BL/6J mice (n=3 per dosing group) were treated with 1 mg/kg of polyamides **1-4** by subcutaneous injection every 3 days, for a cycle of three injections and then sacrificed two days after the final injection (Fig. 4.4A). As in the single dosing experiments, two mice per group were subjected to histopathology analysis and all blood samples were sent for analysis. Mice treated with **1**, **2** and **3** demonstrated no loss in weight or physical morbidities. Two sequential injections of **4** at 1 mg/kg resulted in dramatic weight loss, loss of mobility, and hunched posture within six days (Fig. 4.4B). These mice were promptly euthanized.

A

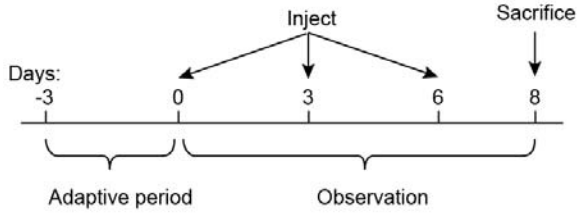

B

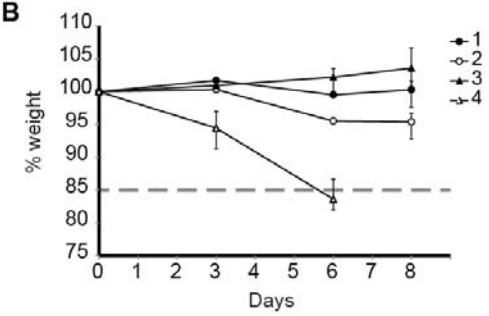

C

Histopathology analysis of mice cadavers after multiple SC injection of polyamide.

		Organ									
Compound	Injections	Cecum	Duodenum	Heart	Ileum	Kidney	Liver	Lung	Pancreas	Spleen	Stomach
1	3					+	+				
2	3					+	+				
3	3										
4	2					+	++			+	

D

Serum chemistry analysis

Compound	Injections	ALT (U/L)	AST (U/L)	T Bili. (mg/dL)	BUN (mg/dL)	Creat. (mg/dL)
1	3	775±167	360±71	0.2	38±1	0.2
2	3	831±136	521±75	0.2	28.5±2.6	0.28
3	3	51±15	56±7.8	0.1	35±4	0.3

Figure 4.4. Experiment set up of multi dose weight curve experiments. **(A)** Male C57BL/6J mice were treated with compound once every three days. Animal weights were then monitored for 9 days. Humane endpoint was defined by visible signs of duress in the animals or weight loss in excess of 15% of original body weight. **(B)** Weight curves of compounds **1**-**4. (C)** Histopathology analysis of sacrificed animals after multiple injections of compounds **1**-**4** at 1mg/kg. + = mild damage, ++ = moderate damage, +++ = severe damage. **(D)** Serum levels of liver damage and kidney damage markers after 3 SC injections of compounds **1**-**3**. Significantly elevated markers are shaded in gray.

Histopathology of these mice treated with polyamide **1** and **2** revealed mild multifocal hepatocellular necrosis and apoptosis in the liver and mild variable tubular attenuation, karyomegaly and epithelial necrosis and apoptosis in the kidney. There was marked hepatocellular necrosis and apoptosis in the liver and hyaline droplet accumulation in the kidneys of animals treated with polyamide **4** (Fig. 4.4C). Because mice treated with **4** did not tolerate two sequential injections at 1 mg/kg, and single dosing resulted in moderate liver and mild kidney damage at 3 mg/kg, we chose not to test this compound further. Consistent with the findings on histopathology, mice treated with **1** and **2** had elevated AST and ALT (Fig. 4.4D). Mice treated with **3** had no

histopathologic lesions consistent with toxicity or alterations in liver and kidney serum markers.

In Vitro Liver Microsomal Stability Assay. Liver pathology was the most striking abnormality and was most severe for **4**. To assess if liver pathology was related to the stability of these compounds, we investigated the metabolic stability of these polyamides to liver microsome isolates. Stability to human and mouse liver microsomes with and without NADPH was tested for polyamides **1-4**. Polyamide **1-3** all demonstrated high stability (>90% intact) after 1 hour incubations (Table S4.2). However, less than 5% of polyamide **4** remained intact after 1 hour incubation with either human or mouse liver microsomes independent of the presence of NADPH.

Liver uptake of Fluorescein-Polyamide Conjugates. To determine if the chemical modifications of the γ-turn corresponding to **1-4** could influence liver uptake of polyamides of otherwise identical structure, we synthesized four polyamide analogous to **1-4,** but with fluorescein isothiocyanate replacing isophthalic acid at the C-terminus (Fig. S4.4). Mice treated with FITC-polyamide conjugate **8**, which has a γ-turn substitution identical to that of **3**, demonstrated less nuclear fluorescence in liver sections than the other FITC-polyamide conjugates (Fig. S4.5). Mice treated with FITC-polyamide conjugate **9**, which has the γ-turn corresponding to **4**, demonstrated the most intense nuclear fluorescence in liver sections.

Cellular uptake and cytotoxicity. To determine the biological activity of **3** in LNCaP cells we first looked for evidence nuclear localization using fluorescein analog **8**. The fluorescein analog of **1**, compound **6**, was used as benchmark. Confocal microscopy of LNCaP cells incubated with 2 μM of **6** or **8** for 24 hr showed robust nuclear localization

(Fig. 4.5A). Viability of LNCaP cells was also reduced in a dose dependent manner by **3**, with the half maximal inhibitory concentration at 2.1±0.3 μM (Fig. 4.5B).

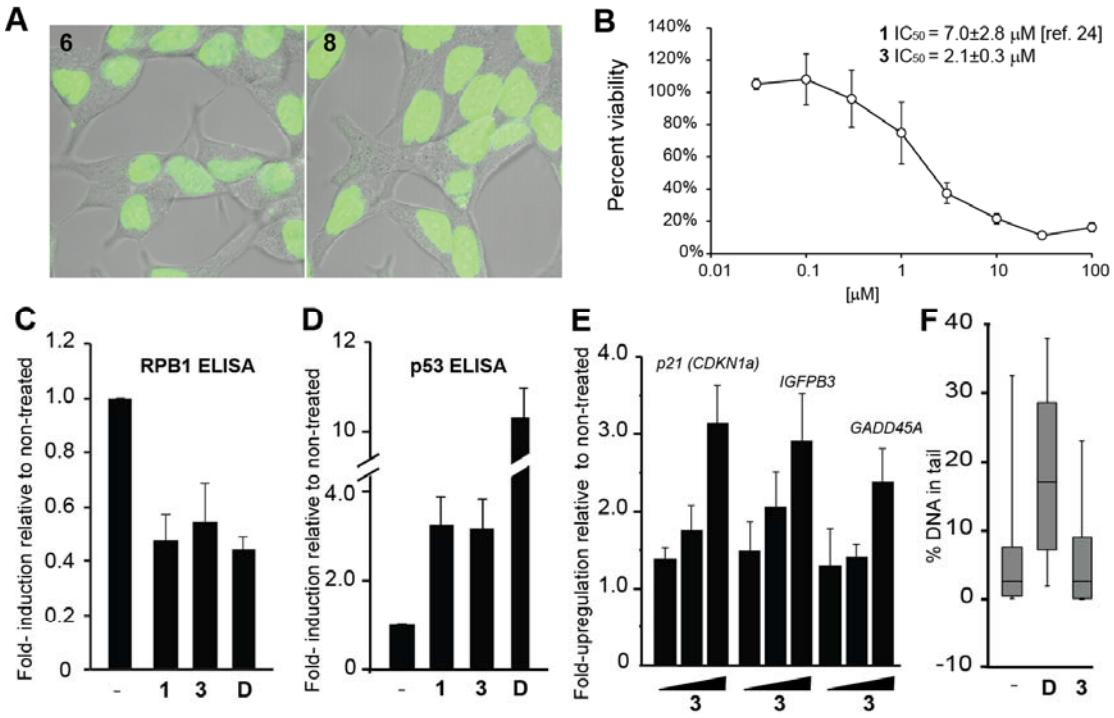

Figure 4.5. Activity of **3** in LNCaP cells. **(A)** Nuclear uptake of **6** and **8**. **(B)** Cellular cytotoxicity of **3** towards LNCaP cells after 72 hr incubation. **(C)** RPB1 protein decreases after treatment with **1** or **3** at 10 μM for 72 hr, or doxorubicin (D) at 1 μM for 24 hr. **(D)** Cellular level of p53 protein increases after treatment **1** or **3** at 10 μM for 72 hr, or D at 1 μM for 24 hr. **(E)** The p53 responsive genes *p21, IGFBP3* and *GADD45A* are induced by **3** in a dose-dependent fashion (concentrations are 1, 3, 10 μM) after 72 hr treatment. **(F)** Alkaline comet assay shows no increase in genomic fragmentation after prolonged incubation with **3** (48hr, 10 μM). Error bars represents 90% range; boxes represents the upper and lower quartiles and median.

Biological characterization. Previously we found **1** to affect the RNA polymerase II holoenzyme, leading to the degradation of the large subunit, RPB1, and increase cellular p53 protein.(24) Similarly, polyamide **3** reduced RPB1 levels when incubated with LNCaP cells at 10μM for 72 h (Fig. 4.5C). The level of p53 protein, as well as the transcripts of several p53 target genes, was also increased after treatment with **3** (Fig. 4.5D-E). In addition, treatment of LNCaP cells with 10 μM of **3** for 48 h did not result in increased DNA damage by the comet assay (Fig. 4.5F).

Antitumor activity. Next, we tested the activity of **3** against LNCaP xenografts in immunocompromised mice. Male NSG immunocompromised mice were engrafted with 2.5 million LNCaP cells. When the tumors reached 200 mm^3 ($0.5 \times L \times W^2$) treatment was initiated. Mice were treated with either **3** (SC, 1 mg/kg in 20% DMSO/normal saline, n=14) or vehicle (20% DMSO/normal saline, n=14) once every three days for a cycle of six injections. The animals were then sacrificed two days after the final injection (Fig. 4.6A). Both groups of animals demonstrated minimal weight loss and no signs of distress during the course of the experiment (Fig. 4.6B). Mice treated with **3** had smaller tumors than those treated with vehicle (T/C = 52.4%) (Fig. 4.6C).

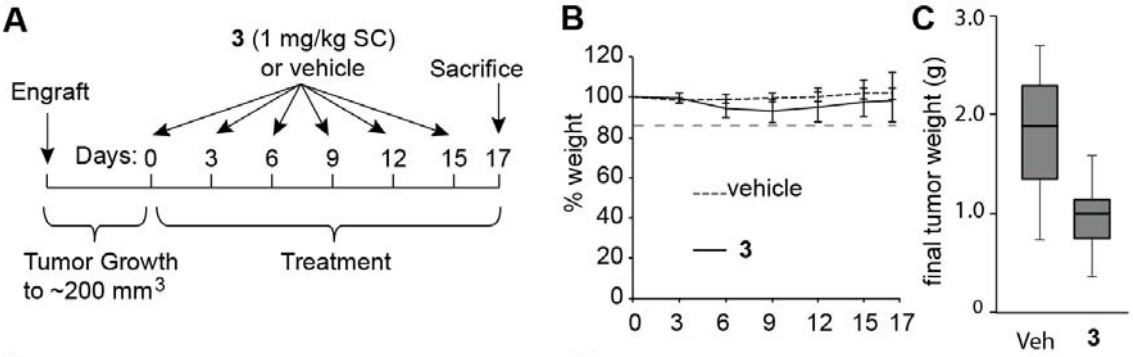

D

Serum Chemistries	
AST (units/L)	80±9
ALT (units/L)	134±56
Total Bilirubin (mg/dL)	0.14±0.05
BUN (mg/dL)	40±5
Creatinine (mg/dL)	0.1

E

Hematology	Pre-	Post-
Total WBC (x1,000/μL)	8±1	9±1
Total RBC (x1,000,000/μL)	10±0.5	11±0.5
HGB (g/dL)	15±1	16±1
Neutrophil (% of WBC)	8±5	10±2
Lymphocyte (% of WBC)	89±5	88±1

Figure 4.6. Activity of **3** against LNCaP Xenografts. **(A)** Timeline of treatment regimen. **(B)** Mouse weights throughout experiment. **(C)** Tumor weights at the experimental endpoint. Error bars represents maximum and minimum; boxes represents the upper and lower quartiles and median. **(D)** Serum chemistry analysis of wild type mice after 6 injections of **3**. Serum levels of AST, ALT, total bilirubin, BUN, and creatinine were found to be within normal limits after compound treatment. **(E)** Hematological analysis of wild type mice after 6 injections of **3**. The levels of white blood cells (WBC), red blood cells (RBC), hemoglobin (HGB), neutrophil, and lymphocytes were not significantly affected by polyamide treatment. Values represent average of 5 animals, errors are s.t.d.

To assess the toxicity of the treatment regimen in healthy animals, male C57BL/6J mice were treated with an identical regimen as the tumor-bearing mice and were sacrificed two days after the final injection. Because the liver and kidney were identified as the target organs of toxicity in our previous study, we assessed relevant serum markers for liver and kidney pathology (Fig. 4.6D). Treated mice demonstrated no elevations in AST, ALT, total bilirubin, creatinine, or BUN. To examine if **3** has an effect on circulating blood counts, whole blood was sampled before treatment and at the time of sacrifice. No significant hematologic changes were noted for the total white blood cell, total red blood cell, hemoglobin, neutrophil, or lymphocyte count (Fig. 4.6E).

4.4 Discussion

Py-Im polyamides interfere with DNA-dependent processes, including transcription, through non-covalent binding to the minor groove and do not result in significant levels of genotoxicity.(24) We believe these characteristics of polyamides may represent a significant advance over current DNA-targeted cancer therapies. We recently reported antitumor efficacy of polyamide **1** against LNCaP xenografts.(24) Our hypothesis is that a new class of oncologic therapeutics could be developed based on the Py-Im polyamide technology platform. However, a more thorough understanding of the effects of selected polyamides in pre-clinical animal models is required.

Although extensive prior work has demonstrated bioavailability of hairpin polyamides in rodents, (28, 35-37) the physiological effects of polyamides in an animal model have not been systematically examined. Based on our lead polyamide **1**, we synthesized three additional polyamides and varied the γ-turn. This chemical change does

not alter DNA target sequence, but affects animal toxicity and tissue distribution in mice.(28)

We find that subtle changes to the γ-turn can dramatically impact systemic toxicity of the selected polyamides in rodents. In line with previously published work, compound **1** caused weight reduction in animals treated at 10 mg/kg but caused no other visible side effects.(28) Compound **4** lead to pronounced deterioration in the animals' condition at 3 and 10 mg/kg. Initially, the toxicity associated with compound **4** was attributed to the acetylation of the primary amine since acetylation generally leads to increased toxicity in cell culture.(27) However the un-acetylated version of **4**, compound **2,** also demonstrated marked toxicity towards the animals while the acetylated version of **1**, compound **3**, showed no adverse effects, suggesting the acetylation of the amine is not the sole contributor to differences in toxicity.

Furthermore, a previous study reported that a cyclic polyamide with a (R)-3,4-diaminobutyric acid turn was more toxic than its hairpin counterpart, which possessed a (R)-2,4-diaminobutyric acid turn. To see if the cyclic version of **1** lead to increased animal toxicity we synthesized **5**. This compound was detectable in the serum after SC injection and was found to have less effect on animal weight than **1**. This suggests the increase in polyamide induced toxicity is associated with the transition of the (R)-2,4-diaminobutyric acid turn to the (R)-3,4-diaminobutyric acid turn.

To identify the cause of animal morbidity we conducted histopathological analysis on sacrificed animals. We found the liver and kidney to be the main organs of pathology for compounds **1**, **2**, **4**, and **5**. Compound **3** caused no detectable organ damage. Liver damage was most pronounced for **2** at 10 mg/kg, and **4** at 3 and 10 mg/kg.

Compound **5** caused moderate damage to both the liver and kidney at 3 and 10 mg/kg. We further confirmed our histopathology results with serum measurements of ALT, AST, total bilirubin, BUN, and creatinine. The liver damage markers ALT and AST were significantly elevated at higher doses of **1**, **2**, **4**, and **5**. Blood urea nitrogen levels were found to be elevated for **2** at 10 mg/kg and **4** at 3 and 10 mg/kg.

In addition to single dose experiments we also examined the effects of **1-4** on animal health after multiple treatments with an injection regimen that was identical to the treatment cycle used in our previous xenograft study.(24) We found compounds **1-3** had minimal effect on animal weight over 3 injections of 1 mg/kg, while compound **4** caused acute distress in the animals after 2 injections. Histopathology and serum marker analysis was able to detect liver and kidney damage in animals treated with all compounds except **3**.

Since the liver is most affected by polyamides, we speculated enzymatic degradation of the compounds may contribute to animal toxicity. To test the stability of compounds **1-4** in the liver we conducted microsomal degradation assays with human and mice liver microsomes. Compounds **1-3** was found to be >90% intact after a 60 min incubation with 1 mg/ml of microsomes. Therefore, the reduced liver toxicity by **3** as compared to **1**, **2**, and **4**, may not be explained on the basis of differing stability to liver microsomes. Interestingly, while **4** was previously reported to be stable against rat and human microsomes,(33) less than 5% of compound **4** was remaining at the end of the assay. This may be explained by the lower amount of enzyme (0.3 mg/ml) used in the previous assay.

The tissue distribution of Py-Im polyamides is largely affected by structure. In our previous pharmacokinetic study we showed **4** had greater localization to the lung, liver, and kidney than **1**. Thus, differences in liver uptake of compounds **1-4** may contribute to the differences in animal toxicity. To visualize nuclear uptake we synthesized fluorescein analogues of **1-4**. Of the four compounds, **8** (the fluorescein analogue of **3**) showed the least amount of nuclear localization, which may explain the apparent lack of animal toxicity.

Polyamide **1** was shown to exert cellular toxicity, in part, through the inhibition of transcription.(24) In line with previous work, polyamide **3**, was also found to affect cellular level of RPB1 and p53, which suggests the cytotoxic effects of **3** also stems from transcription inhibition. Furthermore, no increased DNA fragmentation was observed when cells were treated with **3**, indicating the compound interferes with transcription in a nongenotoxic manner.

In addition to exhibiting similar biological activity in cell culture and having reduced animal toxicity, **3** also demonstrated antitumor activity towards LNCaP xenografts. Tumor-bearing animals and wild type animals were able to sustain 6 injections of **3** without showing any signs of duress. Further characterization of serum chemistries and hematology markers indicates compound **3** is well tolerated by the animals.

In conclusion, we have identified a structural motif that affects the animal toxicity of Py-Im polyamides. The transition of the (R)-2,4-diaminobutyric acid turn to a (R)-3,4-diaminobutyric acid turn significantly increases the animal liver and kidney damage caused by polyamides. Out of the panel of four compounds we have identified

polyamide **3**, which contains the (R)-2-acetylamino-4-aminobutyric acid turn and demonstrates no detectable animal toxicity at 10 mg/kg. This compound behaves similarly to **1** in cell culture, and retains antitumor activity towards LNCaP xenografts. This second-generation hairpin polyamide provides a promising lead for the development of Py-Im polyamides as anticancer therapeutics.

References

1. Jemal A, Center MM, DeSantis C, & Ward EM (2010) Global patterns of cancer incidence and mortality rates and trends. *Cancer epidemiology, biomarkers & prevention : a publication of the American Association for Cancer Research, cosponsored by the American Society of Preventive Oncology* 19(8):1893-1907.
2. Zelefsky MJ*, et al.* (2010) Metastasis after radical prostatectomy or external beam radiotherapy for patients with clinically localized prostate cancer: a comparison of clinical cohorts adjusted for case mix. *Journal of clinical oncology : official journal of the American Society of Clinical Oncology* 28(9):1508-1513.
3. Tendulkar RD*, et al.* (2012) Redefining high-risk prostate cancer based on distant metastases and mortality after high-dose radiotherapy with androgen deprivation therapy. *International journal of radiation oncology, biology, physics* 82(4):1397-1404.
4. Chen Y & Scher HI (2012) Prostate cancer in 2011: Hitting old targets better and identifying new targets. *Nature reviews. Clinical oncology* 9(2):70-72.
5. Li Y*, et al.* (2013) Androgen receptor splice variants mediate enzalutamide resistance in castration-resistant prostate cancer cell lines. *Cancer research* 73(2):483-489.
6. Mostaghel EA*, et al.* (2011) Resistance to CYP17A1 inhibition with abiraterone in castration-resistant prostate cancer: induction of steroidogenesis and androgen receptor splice variants. *Clinical cancer research : an official journal of the American Association for Cancer Research* 17(18):5913-5925.
7. Koumenis C & Giaccia A (1997) Transformed cells require continuous activity of RNA polymerase II to resist oncogene-induced apoptosis. *Molecular and cellular biology* 17(12):7306-7316.
8. Jung Y & Lippard SJ (2006) RNA polymerase II blockage by cisplatin-damaged DNA - Stability and polyubiquitylation of stalled polymerase. *Journal of Biological Chemistry* 281(3):1361-1370.
9. Pommier Y (2006) Topoisomerase I inhibitors: camptothecins and beyond. *Nat Rev Cancer* 6(10):789-802.
10. Mantoni TS, Reid G, & Garrett MD (2006) Androgen receptor activity is inhibited in response to genotoxic agents in a p53-independent manner. *Oncogene* 25(22):3139-3149.
11. Haffner MC*, et al.* (2010) Androgen-induced TOP2B-mediated double-strand breaks and prostate cancer gene rearrangements. *Nat Genet* 42(8):668-U645.
12. Arseneau JC*, et al.* (1972) Nonlymphomatous malignant tumors complicating Hodgkin's disease. Possible association with intensive therapy. *The New England journal of medicine* 287(22):1119-1122.
13. Sun Y*, et al.* (2012) Treatment-induced damage to the tumor microenvironment promotes prostate cancer therapy resistance through WNT16B. *Nat Med* 18(9):1359-+.
14. Dervan PB (2001) Molecular recognition of DNA by small molecules. *Bioorganic & medicinal chemistry* 9(9):2215-2235.
15. Best TP, Edelson BS, Nickols NG, & Dervan PB (2003) Nuclear localization of pyrrole-imidazole polyamide-fluorescein conjugates in cell culture. *Proceedings*

of the National Academy of Sciences of the United States of America 100(21):12063-12068.

16. Olenyuk BZ*, et al.* (2004) Inhibition of vascular endothelial growth factor with a sequence-specific hypoxia response element antagonist. *Proceedings of the National Academy of Sciences of the United States of America* 101(48):16768-16773.
17. Nickols NG & Dervan PB (2007) Suppression of androgen receptor-mediated gene expression by a sequence-specific DNA-binding polyamide. *Proceedings of the National Academy of Sciences of the United States of America* 104(25):10418-10423.
18. Nickols NG, Jacobs CS, Farkas ME, & Dervan PB (2007) Modulating hypoxia-inducible transcription by disrupting the HIF-1-DNA interface. *ACS chemical biology* 2(8):561-571.
19. Raskatov JA*, et al.* (2012) Modulation of NF-kappa B-dependent gene transcription using programmable DNA minor groove binders. *Proceedings of the National Academy of Sciences of the United States of America* 109(4):1023-1028.
20. Nickols NG*, et al.* (2013) Activity of a Py-Im Polyamide Targeted to the Estrogen Response Element. *Molecular cancer therapeutics*.
21. Kielkopf CL, Baird EE, Dervan PB, & Rees DC (1998) Structural basis for G.C recognition in the DNA minor groove. *Nature structural biology* 5(2):104-109.
22. Kielkopf CL*, et al.* (1998) A structural basis for recognition of A.T and T.A base pairs in the minor groove of B-DNA. *Science* 282(5386):111-115.
23. White S, Szewczyk JW, Turner JM, Baird EE, & Dervan PB (1998) Recognition of the four Watson-Crick base pairs in the DNA minor groove by synthetic ligands. *Nature* 391(6666):468-471.
24. Yang F*, et al.* (2013) Antitumor activity of a pyrrole-imidazole polyamide. *Proceedings of the National Academy of Sciences of the United States of America* 110(5):1863-1868.
25. Dervan PB & Edelson BS (2003) Recognition of the DNA minor groove by pyrrole-imidazole polyamides. *Current opinion in structural biology* 13(3):284-299.
26. Dose C, Farkas ME, Chenoweth DM, & Dervan PB (2008) Next generation hairpin polyamides with (R)-3,4-diaminobutyric acid turn unit. *Journal of the American Chemical Society* 130(21):6859-6866.
27. Meier JL, Montgomery DC, & Dervan PB (2012) Enhancing the cellular uptake of Py-Im polyamides through next-generation aryl turns. *Nucleic acids research* 40(5):2345-2356.
28. Synold TW*, et al.* (2012) Single-dose pharmacokinetic and toxicity analysis of pyrrole-imidazole polyamides in mice. *Cancer Chemother Pharmacol*.
29. Puckett JW, Green JT, & Dervan PB (2012) Microwave Assisted Synthesis of Py-Im Polyamides. *Organic letters* 14(11):2774-2777.
30. Belitsky JM, Nguyen DH, Wurtz NR, & Dervan PB (2002) Solid-phase synthesis of DNA binding polyamides on oxime resin. *Bioorganic & medicinal chemistry* 10(8):2767-2774.
31. Nickols NG, Jacobs CS, Farkas ME, & Dervan PB (2007) Improved nuclear localization of DNA-binding polyamides. *Nucleic acids research* 35(2):363-370.

32. Li BC, Montgomery DC, Puckett JW, & Dervan PB (2013) Synthesis of cyclic Py-Im polyamide libraries. *The Journal of organic chemistry* 78(1):124-133.
33. Chenoweth DM, Harki DA, Phillips JW, Dose C, & Dervan PB (2009) Cyclic Pyrrole-Imidazole Polyamides Targeted to the Androgen Response Element. *Journal of the American Chemical Society* 131(20):7182-7188.
34. Raskatov JA, Hargrove AE, So AY, & Dervan PB (2012) Pharmacokinetics of Py-Im Polyamides Depend on Architecture: Cyclic versus Linear. *Journal of the American Chemical Society* 134(18):7995-7999.
35. Nagashima T*, et al.* (2009) Pharmacokinetic modeling and prediction of plasma pyrrole-imidazole polyamide concentration in rats using simultaneous urinary and biliary excretion data. *Biol Pharm Bull* 32(5):921-927.
36. Nagashima T*, et al.* (2009) Determination of pyrrole-imidazole polyamide in rat plasma by liquid chromatography-tandem mass spectrometry. *J Chromatogr B Analyt Technol Biomed Life Sci* 877(11-12):1070-1076.
37. Fukasawa A*, et al.* (2007) Optimization and validation of a high-performance liquid chromatographic method with UV detection for the determination of pyrrole-imidazole polyamides in rat plasma. *Journal of chromatography. B, Analytical technologies in the biomedical and life sciences* 859(2):272-275.

4.5 Supplemental Material

Compound	Chemical Formula	Calculated Mass		Observed Mass
1	C65H76N22O12	[M+H]+	1357.44	1357.86
2	C65H76N22O12	[M+H]+	1357.44	1357.69
3	C67H78N22O13	[M+H]+	1399.48	1399.91
4	C67H78N22O13	[M+H]+	1399.48	1399.36
5	C54H61N21O10	[M+Na]+	1186.5	1186.6

Table S4.1. MALDI-ToF analysis of compounds.

Polyamide	5'- TTGC **TGTTCT** GCAA -3'	
	T_m / °C	ΔT_m / °C
—	61.8 (±0.5)	—
1	74.1 (±0.3)	12.3
2	75.1 (±0.4)	13.3
3	70.1 (±0.2)	8.3
4	74.9 (±0.2)	13.2

Fig. S4.1. DNA thermal stabilization analysis of compounds **1-4.**

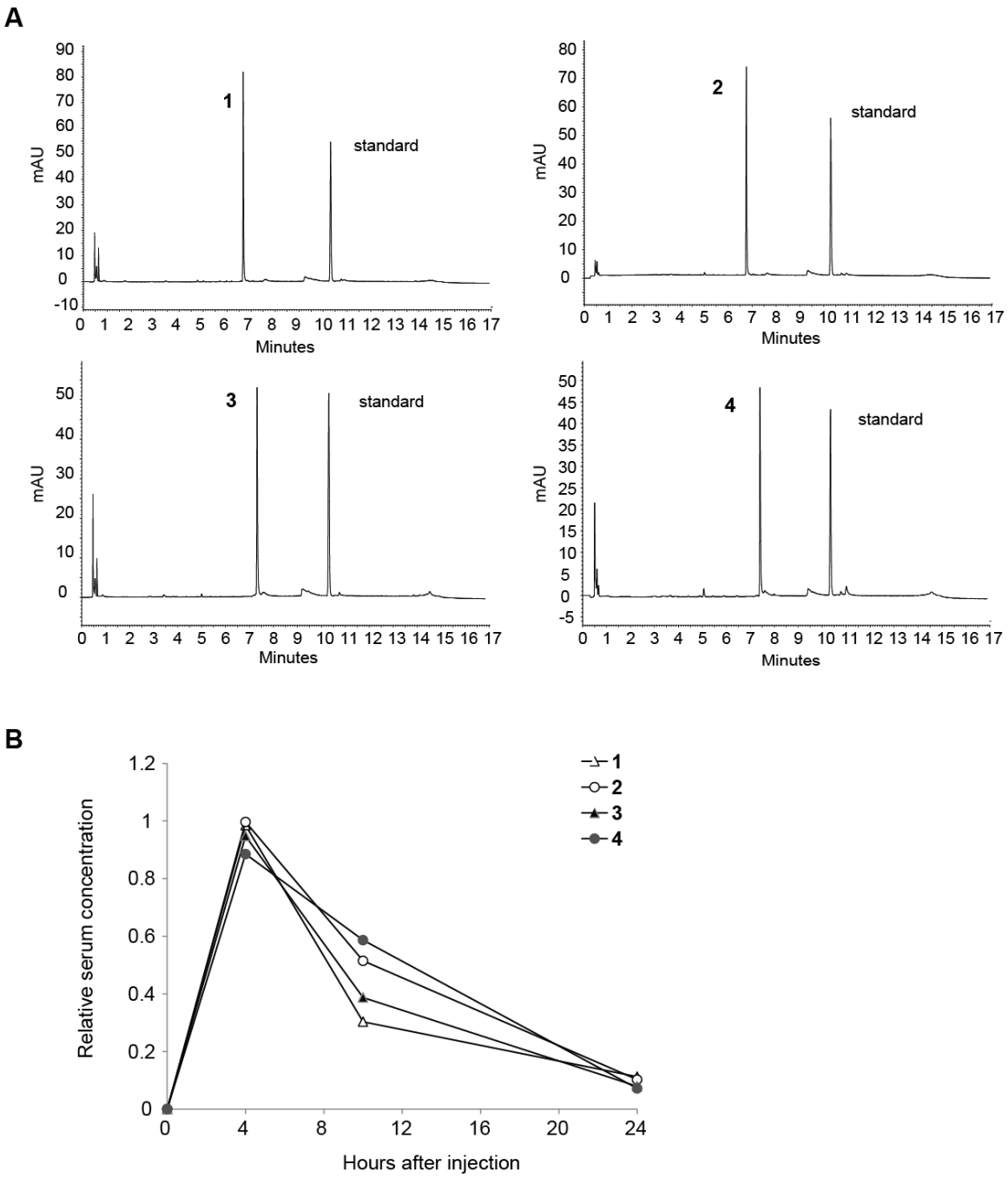

Fig S4.2. **(A)** Analytical HPLC traces of compounds **1**-**4** in the serum 4 hr after injection. **(B)** Relative serum levels of compounds **1**-**4** at 4 hr, 10 hr, and 24 hr after a single subcutaneous injection of each compound at 10 mg/kg.

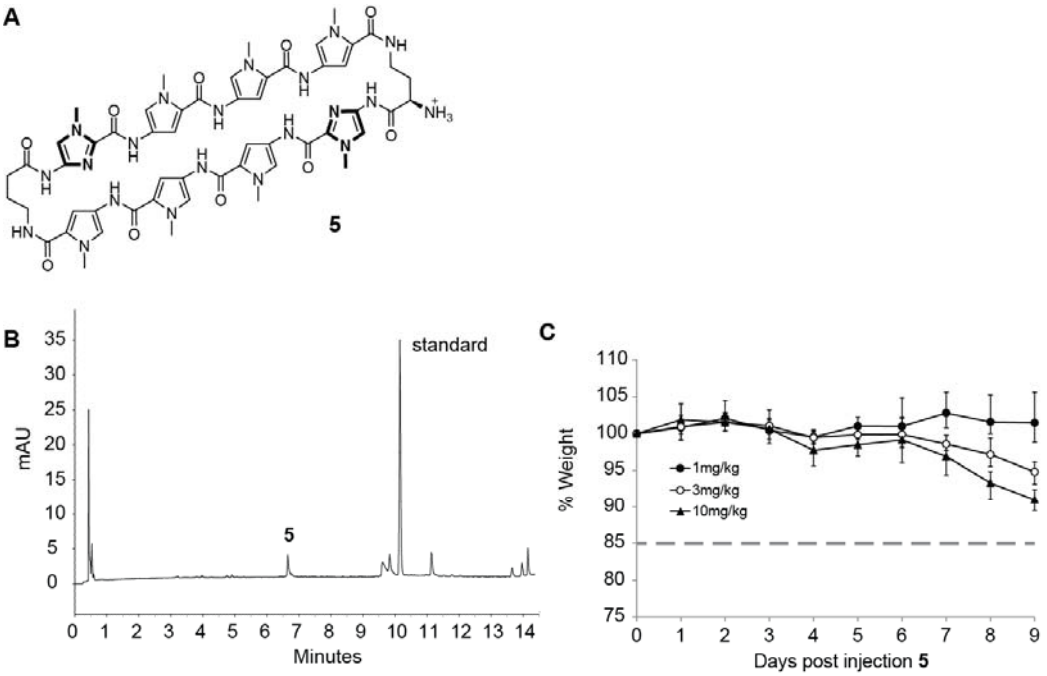

E

mg/kg	ALT	AST	T Bili.	BUN	Creat.
1	189±9.6	103±12	0.13	32±2	0.05
3	809±169	285±33	0.25	38±10	0.18
10	1577±399	615±203	0.3	28.8±8.6	0.18

Fig S4.3. Characterization of a cyclic polyamide targeting the sequence 5'-WGWWCW-3'. **(A)** Chemical structure of compound **5. (B)** Serum circulation of **5** 4 hr after SC injection. **(C)** Changes in animal weights after a single SC injection of **5** at the indicated concentrations. **(D)** Kidney and liver histology of sacrificed animals after 9 days of monitoring. **(E)** Serum chemistry of animals treated with **5**. **Liver:** long gray arrow =hepatocellular apoptosis/necrosis, arrowheads=outline area of bridging hepatocellular necrosis/apoptosis. **Kidney:** short gray arrow=tubular epithelial karyomegaly, long gray arrow=tubular epithelial apoptosis/ necrosis, short black arrow=tubular epithelial mitoses, long black arrow=tubular epithelial attenuation

	Test conc (μM)	Test species	Mean remaining parent with NADPH (%)	Mean remaining parent NADPH-free (%)
Verapamil high metabolism control	1	Human	4.2%	100%
	1	Mouse	1.1%	100%
Warfarin low metabolism control	1	Human	100%	100%
	1	Mouse	100%	100%
1	1	Human	96.9%	92.3%
	1	Mouse	95.2%	96.8%
2	1	Human	91.9%	100%
	1	Mouse	92.4%	100%
3	1	Human	95.3%	94.9%
	1	Mouse	97.3%	100%
4	1	Human	3.0%	3.8%
	1	Mouse	4.0%	4.9%

Table S4.2. Microsomal stability analysis of **1**-**4** in the presence and absence of NADPH. Samples were incubated for 1 hr at 37 °C with 1 mg/ml of human or mouse microsomes.

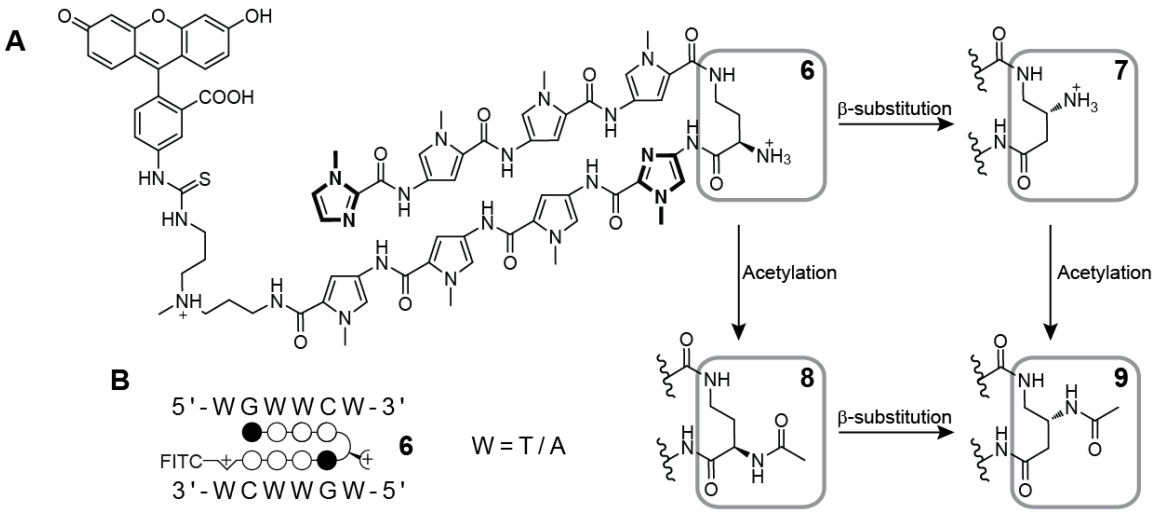

Figure S4.4. Chemical structures. **(A)** Structures of polyamides **6-9.** The compounds only vary by the amino substitution on the g-turn unit. **(B)** The prefered DNA binding sequence of the polyamide core. Polyamide **6** is shown bound to the sequence 5'-WGWWCW-3'. Closed circles represent imidazole units and open circles represent pyrrole units.

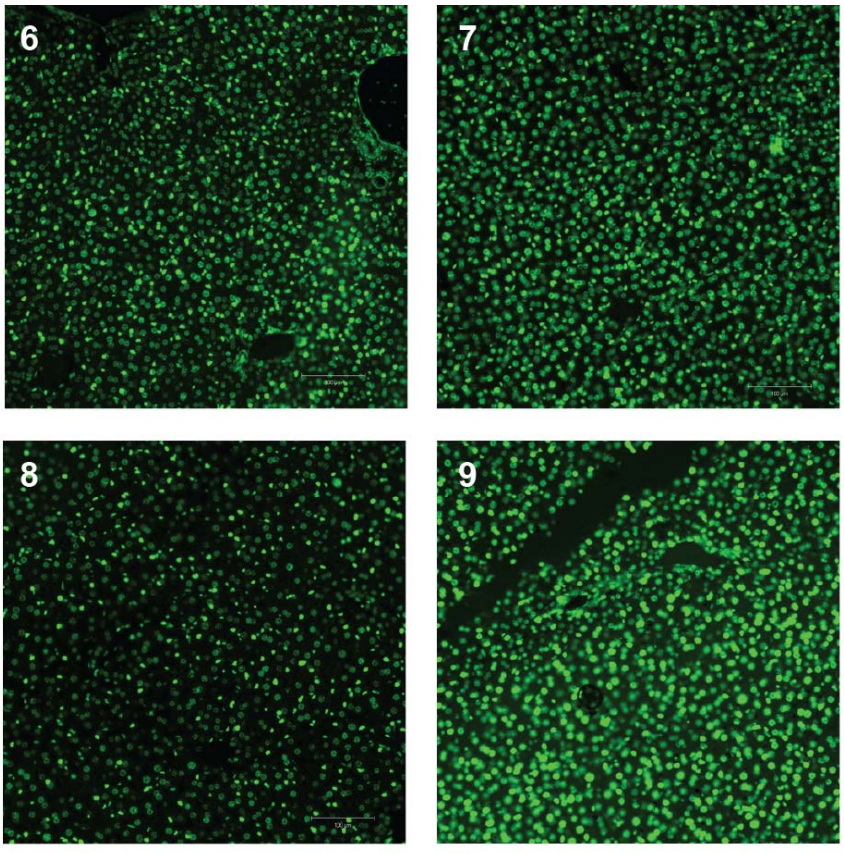

Figure S4.5. Nuclear localization of compounds **6-9** in the liver 24 hr after SC injection